MAGIC-TDAS 07-02
070417 / J. Rico

Observations of the black-hole microquasar Cygnus X-1 with MAGIC during cycle-II

Javier Rico and Juan Cortina

Institut de Física d'Altes Energies (IFAE)
Edifici Cn. Universitat Autònoma de Barcelona
08193 Bellaterra (Barcelona) Spain

Abstract

We present the results of the analysis of Cygnus X-1 observations carried out during 26 good nights from June to November 2006, for a total effective time of 40.0 hours. The analysis optimization is performed using Crab nebula observations from the same period, reaching a sensitivity of 2.22% (2.91%) of the Crab flux above 600 (200) phe. Searches for steady gamma-ray signals yield no positive result and upper limits at 1.3% (1.9%) Crab flux above 410 (130) GeV can be established. We have also performed a phase-folded analysis, using the orbital period of 5.6 days and the inferior conjunction of the companion star as phase 0. We establish flux upper limits of about 4% the Crab flux for all 0.1-width phase bins except for the bin 0.9-1.0, where we see a $\sim 4\sigma$ evidence of a signal. The data in this phase bin correspond to a single observation night (27/09/2006, MJD=54002.88). We search for signals also on a day-by-day basis, establishing limits between 5 and 10% Crab for all of them except for the aforementioned observation night. We have defined a systematic, unbiased procedure to search for fast-varying signals and found a 4.8σ signal for the observation period MJD=54002.93-54002.96. We have tried to increase the significance by adding lower SIZE bins and by using a larger sample for background estimation. We show that the first method is not reliable and using the second one we obtain a significance of 4.9σ. The differential spectrum of the detected signal is well fitted by an unbroken power law with spectral index $\alpha = -3.4$ and a normalization at 1 TeV of about 10% Crab. The distribution of excess events is compatible with that expected for a point-like source, and its localization is compatible with the position of Cygnus X-1. The nearby jet-powered radio nebula is excluded as the region produging the gamma-ray signals. Furthermore, we examine the correlation between the found signal and X-ray observations by Swift, RXTE-ASM and INTEGRAL. All these three detectors observed a large (historical in the case of INTEGRAL) increase in the observed flux of Cygnus X-1. MAGIC gamma-ray signal occurs between 1 and 2 hours before one of the X-ray peaks detected by Swift.

1 Introduction

Cygnus X-1 is the first binary system where dynamic evidence for a black hole was found [1]. This source is also the brightest persistent high mass X-ray binary in the Galaxy, radiating a maximum X-ray luminosity of a few 10^{37} erg s^{-1}. The mass of the black hole is 10 solar masses and the companion star is an O9.7 supergiant. The distance to the system is 2.1 kpc. The orbit of the system is low eccentric or circular, with a period of 5.6 days and an inclination of 30°. The source displays high-soft and low-hard spectral states, spending most of the time in the low-hard. In such a state steady compact jets are produced and quenched, a penomenon thought to be unrelated to the inner radius of the accretion disk [2], giving support to a hard X-ray emitting corona at the base of the jet. VLBA observations of Cygnus X-1 showed a bright core with a slightly extended structure of about 15 mas (40 AU) [3]. Furthermore, it has been recently discovered a large-scale ring-like radio structure of about 5 pc in diameter (8 arc-min) that appears to be produced by the prolonged action of the jet on the ambient medium [4]. An intrisic jet velocity of $\leq 0.3c$ has been recently deduced [5]. The radio emission generally maintains a stable level and flat spectrum. COMPTEL, on board of the CGRO, did detect Cygnus X-1 in the 1-30 MeV range several times [6]. Unfortunatelly, EGRET performed rather few observations of Cygnus X-1 and did not detect it. Only quite loose upper limits to the $\sim$ 100 MeV flux are available [7]. As far as we know, there are no publicly available results on TeV observations of Cygnus X-1.

MAGIC has observed Cygnus X-1 for about 40 hours during cycle II [8], in wobble mode. Here we present the results of the analysis of the acquired data. We start by presenting an extensive description of the analysis and statistical treatment of the signal (Sections 2 and 3). After that, we show the results obtained for Cygnus X-1 (Section 4) on the search for steady, periodic and fast-varying gamma-ray signals. The positive result is sudied deeper and compared with contemporaneous results obtained by X-ray satellites. Finally, we present our conclusions in Section 5.

2 Data samples

Data from Crab Nebula dark observations in wobble mode were used to assess the sensitivity of the analysis, as well as to compute the gamma-ray fluxes from Cygnus X-1, as will be explained below. Table 1 summarizes the analyzed Crab Nebula data sets. This data sample has been chosen in order to fit as much as possible the zenith angle distribution of the Cygnus X-1 observations. The distribution of the zenith angles is shown in Figure 1.

Period	Dates	Zenith [deg]	Obs. time [hours]	Sel. time [hours]
46	Sep 21,24,25	12-32	3.7	3.7

Table 1: Details of Crab Nebula observations used in the present analysis. Shown are, from left to right: the period and date of the different observation nights, covered zenith angle range, total observation time, observation time after and data quality selection criteria.

Cygnus X-1 was observed for a total of 46.2 dark hours in wobble mode. Out of them 6.2 hours were discarded due to quality cuts based on the trigger and cleaning rates (see Figure 2). Details on the data sample can be found in Table 2. The observations were scheduled for zenith angles below 30°. However, for the latter observation periods it became necessary to extend the zenith angle limit up to 35° in order to be able to acquire all the assigned time. The distribution of zenith angles for the whole considered data sample is shown in Figure 1.

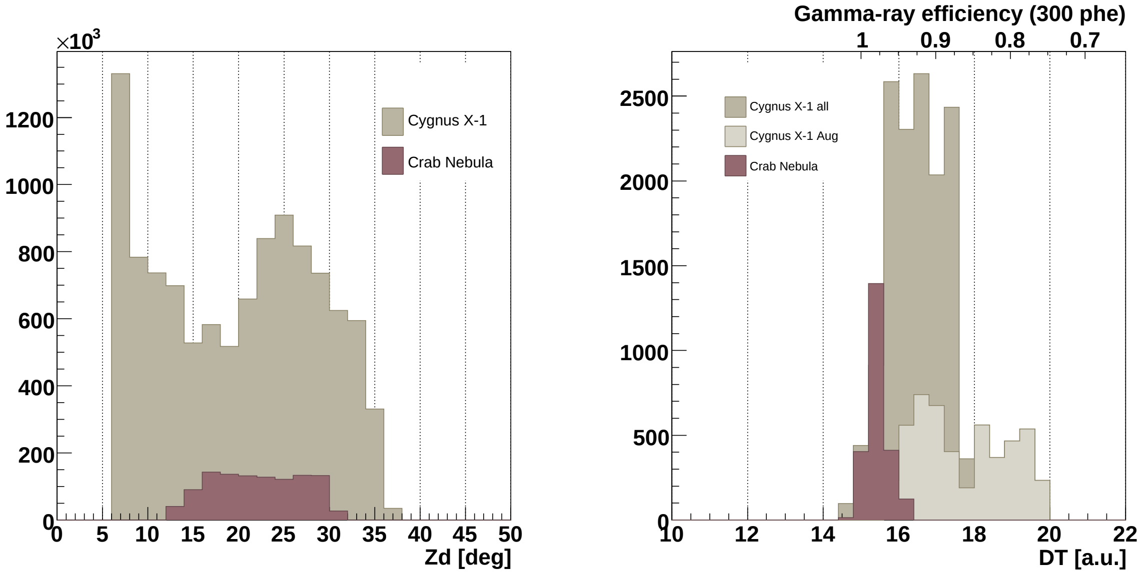

Figure 1: Zenith angle (left) and discriminator threshold (rigt) distributions for Crab Nebula and Cygnus X-1 observations.

Period	Dates	Zenith [deg]	Obs. time [hours]	Sel. time [hours]
43	Jun 30, Jul 1	25-29	0.3	0.2
44	Jul 25-26	7-30	1.9	1.0
45	Aug 16-22	5-30	15.5	11.9
46	Sep 17-20, 23, 25-29	5-35	19.6	19.1
47	Oct 12-15, 21-12	20-35	5.9	5.3
48	Nov 10,11,14,18,19	24-36	3.0	2.5
Total		5-36	46.2	40.0

Table 2: Details of Cygnus X-1 observations used in the present analysis. Shown are, from left to right: the period and date of the different observation nights, covered zenith angle range, total observation time and observation time after data quality selection criteria.

Although the source was observed in dark (no moonlight or twilight) conditions, the distribution of mean discriminator threshold (DT) values (see Figure 1) shows that the DT's were, probably due to the presence of a 3.9 magnitude star in the field of view (Cyg-η at $0.26°$ from Cygnus X-1), higher than the nominal value, especially during August 2006. This results in a loss of gamma-ray collection efficiency with respect to what we measure from the Crab Nebula. The value of the gamma-ray efficiency for 300 phe (computed from [9]) is shown as an example in the upper axis of the figure. A gamma-ray efficiency loss of up to 25% is expected for 300 phe showers. This fact will have to be properly taken into account when computing gamma-ray fluxes and limits.

Apart from the black hole, the large-scale ring-like structure [4], which is though to be produced by the interaction of the particles accelerated in the jet with the surrounding matter is another natural candidate to be a gamma-ray emitter. This ring-like structure is at a distance of $0.13°$ degrees from the black hole, and hence can be resolved by MAGIC. This makes especially important having under control the possible mispointing during the observation. Figure 3 shows the zenith and azimuth

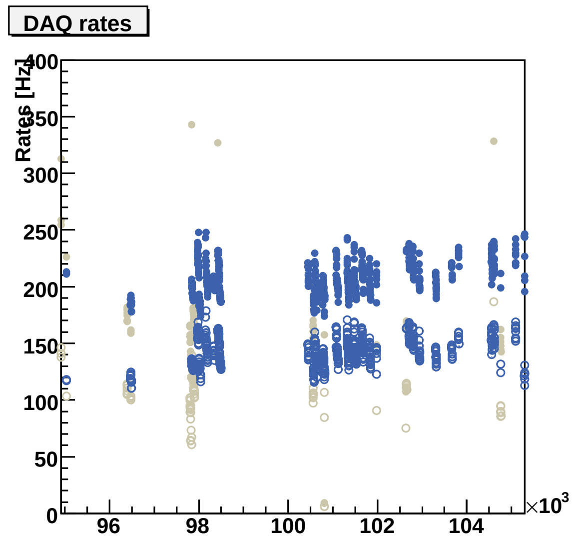

Figure 2: Event rate before (solid) and after (empty) image cleaning as a function of the run number (left) and of the cosine of the zenith angle (right). In dark blue (light brown) the runs considered (discarded) for further analysis.

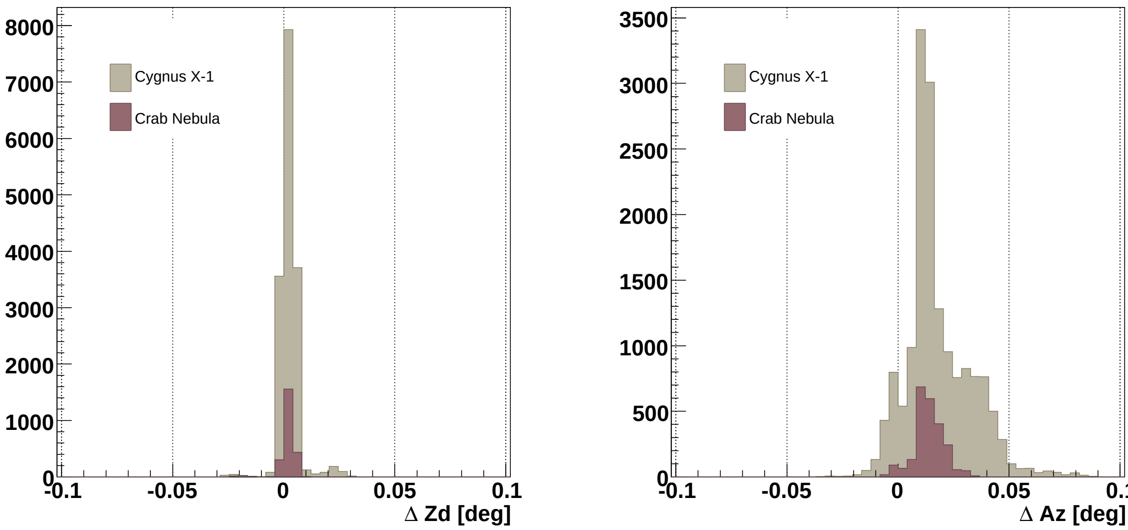

Figure 3: Zenith angle (left) and azimuth (right) deviations measured by the Starguider system during the Crab Nebula and Cygnus X-1 observations.

deviations measured by the Starguider system during the observations analyzed in this work. The measured values are always well below half the size of a pixel and hence no further correction for mispointing has been applied.

In addition, we have used a sample of Monte Carlo (MC) simulated gamma-ray events to train the algorithms for gamma-hadron separation, determination of the primary arrival direction and energy estimation, as well as to determine the energy and angular resolutions. The standard sample of simulated gamma-ray showers, observed in wobble mode and zenith angles below 30° were reprocessed using the correct gains and noise after the installation of the splitters for the new MUX FADC's and the correct value of the optical point spread function [11]. The total sample was divided into two equally-sized, independent subsamples for training and testing of the algorithms, respectively. The standard sample of high-energy MC gammas (with the energy input distribution being a power law with index -1) was used to train and test the energy estimation algorithm.

3 Data Analysis

3.1 Calibration and data reduction

The calibration of the signals and image cleaning were performed by the analysis programs running at La Palma at the time of the observations (Mars v0.12.3, signal extracted with Digital Filter, (10,5) phe. absolute cleaning levels.

After that, runs with too high or too low event rate are removed as explained in the previous section. Also, the following list of quality selection pre-cuts is applied:

- SIZE>80 phe
- LEAKAGE<0.1
- Number of core pixels>5
- Number of islands<2
- Spark cut: $\log_{10}$(CONC) < -0.36 $\log_{10}$(SIZE)+0.618

The distribution –after quality pre-cuts– of the relevant Hillas variables (SIZE, WIDTH, LENGTH, M3LONG, CONC) as well as of the angular distribution of the center of gravity of the images are shown in Figure 4. The agreement between the different analyzed samples is quite good. A comparison between the distributions made for individual observation nights yields the same level of agreement.

We use the standard algorithms for gamma-hadron separation, energy estimation (Random Forest) and determination of the primary arrival direction (DISP). The training is carried out using osteria and the computation of the variables using melibea, both from the official release Mars v0.13.0. For the training, half of the MC samples, –randomly selected– is used, while the other half is left for test of the methods' performance. For gamma-hadron separation, also a sample of randomly selected events from Cygnus X-1 observations is used. The following variables have been used to train the different algorithms:

- Gamma-hadron separation: $\log_{10}$(SIZE), WIDTH, LENGTH, $\log_{10}$(SIZE)/(WIDTH×LENGTH), M3LONG×sign(X cos(DELTA)+ Y sin(DELTA)), CONC.
- Energy estimation: $\log_{10}$(SIZE), WIDTH, LENGTH, $\log_{10}$(SIZE)/(WIDTH×LENGTH), CONC, LEAKAGE, ZD (zenith angle).
- Primary incoming direction:
  DISP = a(SIZE) + b(SIZE) × WIDTH/(LENGTH+η(SIZE)×LEAKAGE),
  where a, b and η are functions of SIZE and optimized with MC to yield the best angular resolution.

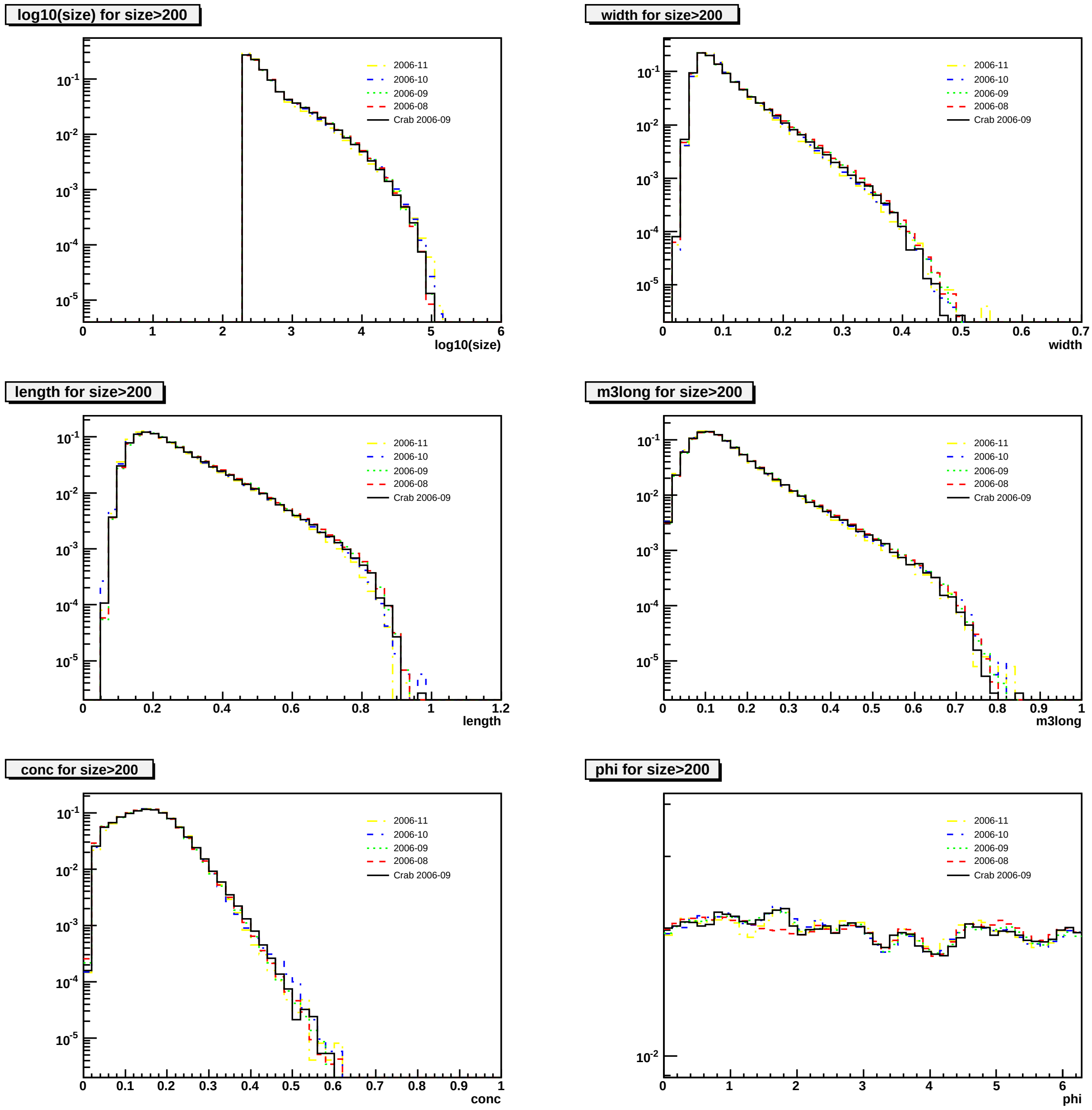

Figure 4: Distribution of the variables relevant for this analysis (separated by month) for Cygnus X-1 and Crab Nebula observations, after data quality cuts. All distributions are normalized by the number of entries and are for a lower cut SIZE>200 phe. From left to right and top to bottom: log10(SIZE) (with SIZE in phe), WIDTH, LENGTH, M3LONG (deg), CONC and PHI, where the first five are defined in the standard way and PHI is the angle of the center of gravity of the shower with respect to the x-axis, and gives an idea of the level of the inhomogeneity of the camera.

The performance of the three algorithms are shown in Figure 5, 6 and 7, respectively.

The Q-factor (Figure 5) increases as expected with the energy, reaching values as high as 27. For all the energy bins the optimal HADRONNESS cut is below 0.15. We can observe also a lack of hadron statistics for the proper determination of the optimal cut and Q-factor at the highest energy bins. However, this does not represent any practical problem since the actual HADRONNESS cut

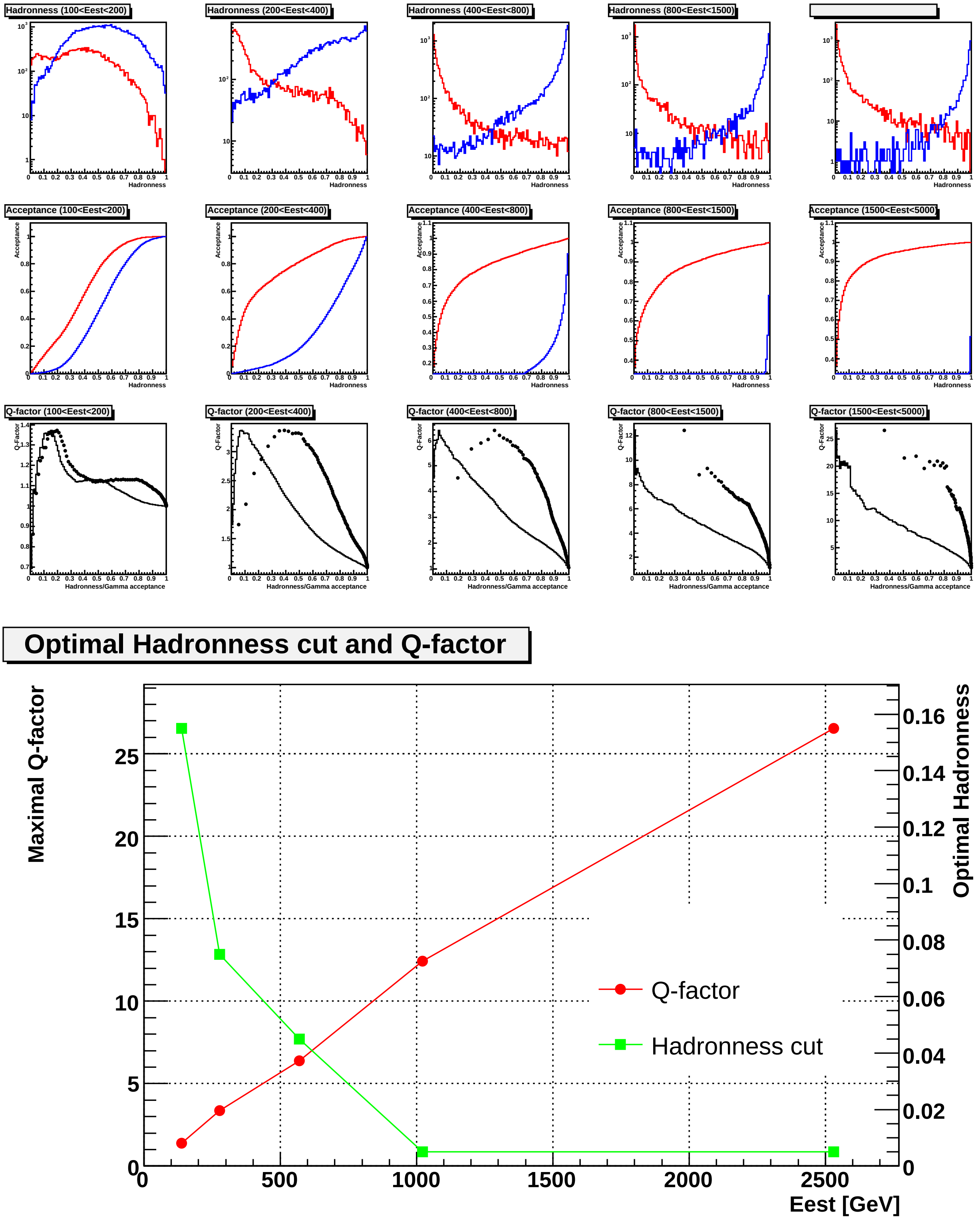

Figure 5: Performance of the gamma-hadron separation algorithm. From top to bottom: HADRONNESS distributions for MC gamma (red) and hadron (blue) events in different Estimated energy bins; gamma (red) and hadron (blue) acceptance as a function of the hadronness upper cut; Q-factor as a function of the HADRONNESS cut (line) and the gamma-ray efficiency (dots); optimal HADRONNESS cut (green) and associated Q-factor (red) as a function of the estimated energy.

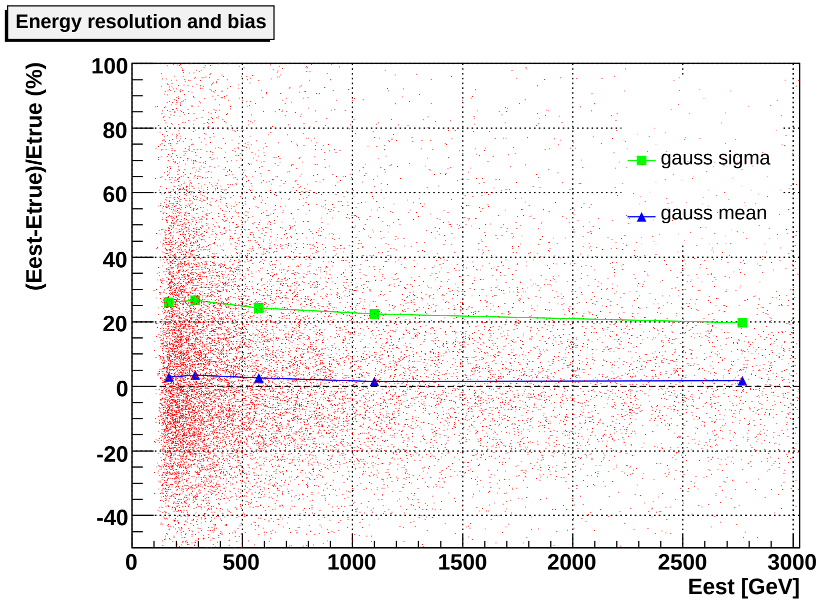

Figure 6: Energy resolution (green) and bias (blue) as a function of the estimated energy computed from MC simulated gamma-ray events (test sample). The values are obtained from the σ and mean of a Gaussian fit to the distribution of $(E_{\mathrm{est}} - E_{\mathrm{true}})/E_{\mathrm{true}}$, whose values for the individual events are shown as red points. A cut HADRONNESS<0.1 has been applied.

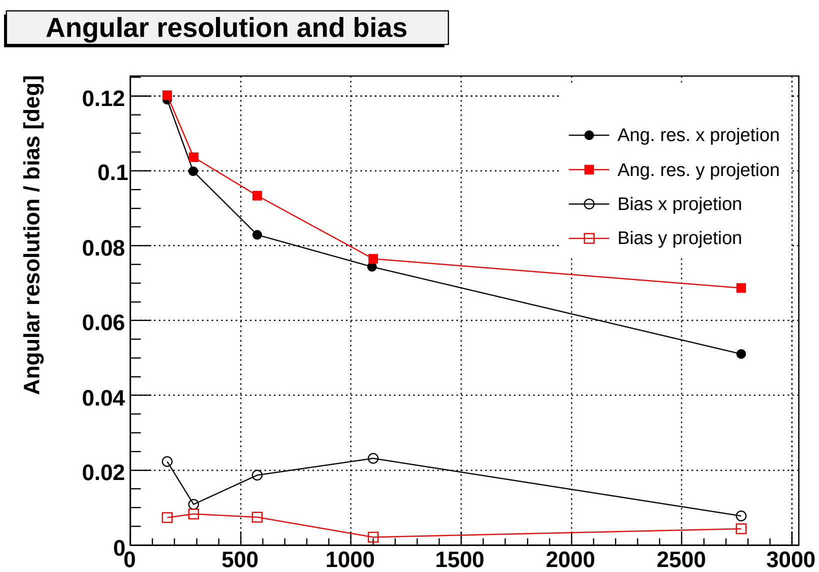

Figure 7: Angular resolution (solid markers) and bias (open markers) as a function of the estimated energy. The values are obtained from the σ and mean of a Gaussian fit to the distribution of reconstructed incoming directions for a the test MC sample. The difference between the x and y directions comes from the fact that the real incoming direction is $(x, y) = (0.4°, 0)$ (in camera coordinates). A cut HADRONNESS<0.1 has been applied.

and sensitivity will be computed by analyzing a Crab sample.

The energy resolution (Figure 6) decreases with the energy and ranges from 25 to 20%, with a bias raging from 4 to 1%

The angular resolution (Figure 7) is well below 0.12° for showers above 100 GeV. There is a non negligible bias in the determination of the primary incoming direction in the along the x axis. This is due to the fact that the real incoming direction is $(x, y) = (0.4°, 0)$ (in camera coordinates). In real experimental conditions, and given that two symmetric wobble positions are observed alternatively and for approximately similar amount of time, the bias will produce an additional contribution to the total angular resolution. This contribution adds quadratically with the intrinsic angular resolution and hence is completely negligible for this study.

3.2 Background estimation

The background recorded in a given position camera position (x, y) can be estimated from n symmetric positions:

$$(x_i, y_i) = R\left(\frac{2\pi i}{n+1}\right)(x, y) \qquad i = 1, ..., n \tag{1}$$

where $R(\phi)$ is the rotation matrix by an angle ϕ, and n has to be such that

$$r \sin\left(\frac{\pi}{n+1}\right) > \theta_{\rm cut} \tag{2}$$

where $r = \sqrt{x^2 + y^2}$; and $\theta_{\rm cut}$ is the radius of the region around (x, y) integrated for signal/background computation.

For an hexagonal camera as that of MAGIC, $n = 1$, 2 or 5. During wobble-mode observations, the nominal distance of the source to the camera center is $r_0 = 0.4°$. This allows to use $n = 5$ points (*anti-source* regions) for background estimation. The statistical error on the background estimation is proportional to $n^{-1/2}$, so one should always use the maximum possible number of symmetric positions.

Let the coordinates of the source be (x_0, y_0). From equation 1 we can compute the coordinates (x_i, y_i) of the n anti-sources. Let the incoming direction reconstructed for a given event be (x, y). We can compute the following $n + 1$ angular distances:

$$\theta_i = \sqrt{(x - x_i)^2 + (y - y_i)^2} \qquad i = 0, ..., n \tag{3}$$

Signal candidate events are defined by the cut $\theta_0 < \theta_{\rm cut}$, and background events by $\theta_i < \theta_{\rm cut}$, for $i = 1 \cdot n$. The normalization factor between signal and background events is $1/n$. $\theta_{\rm cut}$ is determined from Crab Nebula analysis by optimization of the sensitivity. Equation 2 ensures that a given event can be considered either as a signal or as a background candidate, but never as both.

Sky-maps showing the number of excess events around the source candidate position are produced in order to check for possible problems in background determination or mispointings and also to determine the exact position and extension of an eventual gamma-ray source. Let the reconstructed incoming direction for a given event be (x_0, y_0), and $(x_i, y_i)\,(i = 1, ..., n)$ the symmetric positions obtained using Equation 1. The sky-map is the 2-dimensional distribution of (x_0, y_0) positions, subtracted the sum of the distributions of (x_i, y_i) where each entry is weighted by $1/n$, with n the maximum value respecting the hexagonal symmetry and Equation 2 for $r = \sqrt{x_0^2 + y_0^2}$ and $\theta_{\rm cut}$ larger than the angular resolution. In our analysis we use $\theta_{\rm cut} = 0.18°$ for sky-maps, well above the angular resolution for all energy values.

The following considerations have to be taken into account when computing the sky-map:

- For events close to the camera center such that $r < \theta_{\rm cut}$, condition 2 cannot be fulfilled. These events are not used in the sky-map. This does not result in "holes" in the sky-map thanks to the fact that the same region of the sky is observed off-center for the complementary wobble position.

- Events closer than $\theta_{\rm cut}$ to the nominal source position are not used in the (x_i, y_i) distributions since they are *a priori* suspected to contain signal events. To compensate for these missing events, those that are closer than $\theta_{\rm cut}$ to one of the nominal anti-sources (obtained from applying equation 1 to the nominal source position) are weighted by $1/(n+1)$. This also applies to any other region in the sky *a priori* suspected to contain signal events.

- Events for which r is such that $n = 1$ and the event is closer than $\theta_{\rm cut}$ to the anti-source position are not used for signal estimation since no background estimation is possible (due to the first exception rule). This does not happen if the nominal source is at a distance r_0 such that $r_0 \sin \pi/3 \geq \theta_{\rm cut}$, as in the case of MAGIC wobble observations and for the value of $\theta_{\rm cut}$ used in this analysis.

This method produces reliable sky-maps with no need of a background model, since background distribution is computed from the data themselves. However, the drawback is that the method is not suited for field of views containing very extended sources or sources at unknown positions.

3.3 Statistical treatment

Let $N_{\rm on}$ be the number of events surviving all analysis cuts, namely quality, HADRONNESS and θ_0 (see Equation 3) cuts. Let $N_{\rm off}$ be the number of events surviving quality, HADRONNESS and θ_i $(i = 1, ..., n)$ cuts. The observation time T is computed as the sum of the differences between run initial and final times for all runs considered. From the previous quantities we can compute the following ones:

- Number of excess events:

$$N_{\rm excess} = N_{\rm on} - \frac{1}{n} N_{\rm off} \tag{4}$$

- Error in the number of excess events:

$$\Delta N_{\rm excess} = \sqrt{N_{\rm on} + \frac{1}{n^2} N_{\rm off}} \tag{5}$$

- Significance (S): computed using Li and Ma prescription (Equation 17 from [12]) with $\alpha = 1/n$, and given in Standard Deviations (SD) units.

- Post-trial chance probability: Li and Ma prescription ensures that S is Gaussian distributed with null mean and unity standard deviation, for the no-signal case. Therefore, the chance probability of obtaining, after a single measurement, a significance equal or higher than S_0 is given by:

$$P(S \geq S_0) = \frac{1}{2}\left(1 - \mathrm{erf}\left(\frac{S_0}{\sqrt{2}}\right)\right) \tag{6}$$

  In general, after m measurements (trials), the probability of obtaining at least one value above S_0 is the complementary probability to obtaining all values below S:

$$P(S_{i \in [1,m]} \geq S_0) = 1 - (1 - P(S \geq S_0))^m \tag{7}$$

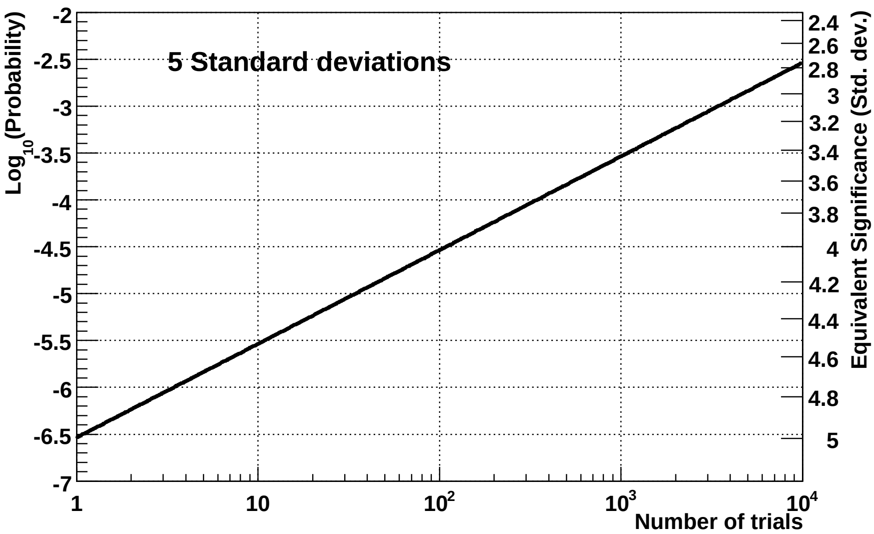

Figure 8: Chance probability of obtaining at least one value at 5 SD or larger, as a function of the number of trials, for a Gaussian distributed estimator. The right axis shows the value of the number of SD corresponding to the probability on the left axis and only one trial.

Figure 8 shows the chance probability of obtaining at least one value at 5 SD or larger, as a function of the number of trials, for a Gaussian distributed estimator. Also shown is the value of the number of SD corresponding to the probability and only one trial. This value is often referred to instead of the probability, and is named post-trial significance.

- Excess rate:
$$R \equiv \frac{dN_{\text{excess}}}{dt} = \frac{N_{\text{excess}}}{T} \tag{8}$$

- Sensitivity (from Crab Nebula observations). It is defined as the minimum integral flux (assuming the same spectral shape as for the Crab Nebula) detectable with a significance of 5 standard deviations in 50 hours of observations:
$$s = 5\sqrt{\frac{T}{50}}\frac{\sqrt{N_{\text{off}}/n}}{N_{\text{excess}}} \tag{9}$$
for T expressed in hours.

- Gamma-ray average efficiency due to the DT values (ϵ): we follow the prescription from [9, 10]. We note that, due to the splitters installed for the MUX FADC's, the DT unit used in the TDAS note is 2.5 times the one corresponding to the data analyzed, and that the nominal DT is 15 a.u. instead of 35. For every event of a given SIZE and acquired under a given value of DT, equations 2 and 5 from [9, 10] allow us to compute a gamma-ray efficiency. The average efficiency is the mean efficiency over the N_{on} events surviving all signal selection cuts.

- Confidence intervals: following the prescription from Rolke [13]. Out of the various methods proposed by the authors, we adopt the one that considers a Gaussian distribution both for the background –which is a good approximation for all considered cases–, and the signal efficiency. The signal efficiency is coming from DT values different from the nominal one, and is obtained as described in the previous paragraph. The σ of the efficency is the quadratic sum of a fixed 10% from day-to-day fluctuations as shown in [9] plus the relative statistical error in the determination of the Crab Nebula flux.

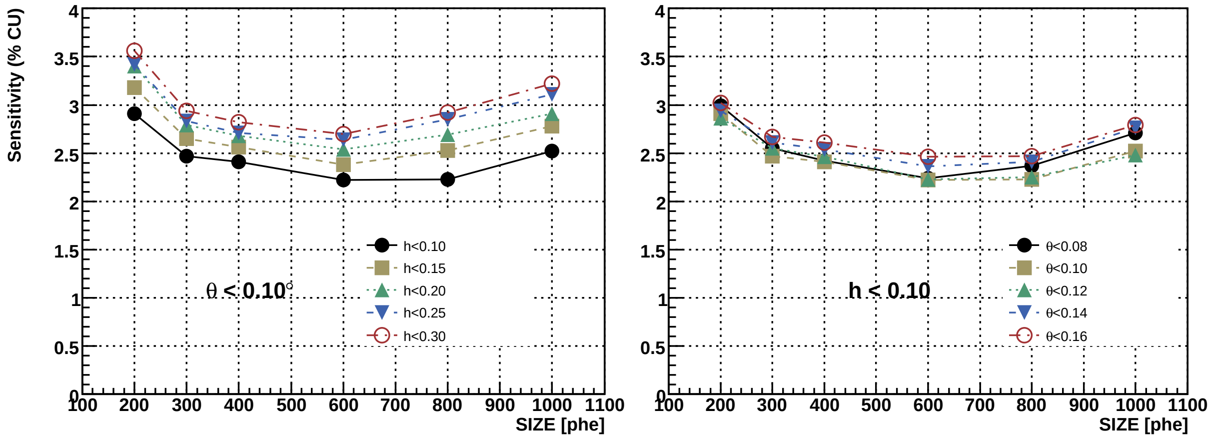

Figure 9: Integral flux sensitivity as a function of the lower SIZE cut for $\theta < 0.10°$ for different HADRONNESS cuts (Left); and HADRONNESS<0.10 for different θ cuts (Right).

3.4 Search for fast varying signals

In order to look for fast varying signals we adopt the following procedure. First, we look for signals on each observation night independently and compute, using LiMa formula and Equation 7, the pre-trial and post-trial significances for each sample. The number of trials is the number of observation nights. After this we follow an iterative process: the different samples are ordered by decreasing significance, starting from the highest significance sample. Following this order, we compute the maximum significance we would obtain (pre- and post-trial with the number of trials increased by 1 with respect to the previous considered case) if we would split the sample into two and all signal was concentrated in one of the two obtained subsamples. This forseen maximum significance gives us an idea about whether it is worth to perform such a sample split. We ask for more than 5 SD pre-trial and 4 SD post-trial to define a split as worthwhile. The procedure is applied until we find the first sample for which the splitting is not worthwhile. In the next step, it is applied to all the obtained by splitting subsamples, following the same rule.

This method provides an unbiased estimate of the timescale of the signal variations while keeping low the number of trials, so that the post-trial probability is not significantly spoiled.

3.5 Analysis sensitivity

The analysis cuts, namely the HADRONNESS and θ cuts, are optimized using data from Crab nebula observations (see Section 2) to yield the best integral sensitivity. In this analysis we have used SIZE-independent HADRONNESS and θ cuts. The sensitivity is evaluated for different lower SIZE cuts, namely 200, 300, 400, 600, 800 and 1000 phe. The probed HADRONNESS lower cuts are 0.10, 0.15, 0.20, 0.25 and 0.30; for the θ cut we try 0.08, 0.10, 0.12, 0.14, 0.16 and 0.18 degrees. First we fix the cut on θ to 0.10° and optimize the cut on HADRONNESS (see Figure 9 left). Then, using the optimal obtained value we vary the cut on θ (see Figure 9 right). The optimal values, used as analysis cuts, are:

$$\begin{aligned} HADRONNESS &< 0.1 \\ \theta &< 0.1^\circ \end{aligned} \tag{10}$$

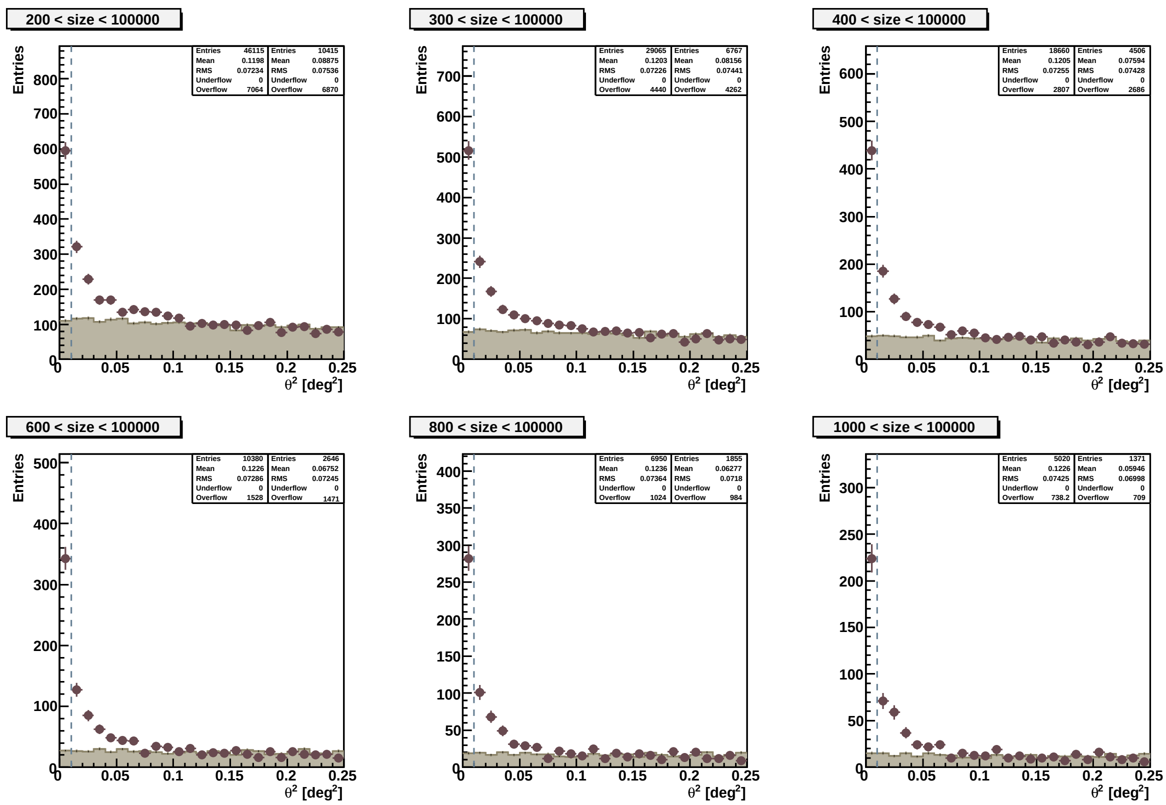

Figure 10: θ^2 distributions after HADRONNESS cut and for the different considered SIZE lower cuts, for the reference Crab Nebula sample. The vertical-dashed lines show the θ^2 cut applied in the analysis to optimize the sensitivity.

The distributions of θ^2 after HADRONNESS cut are shown in figure 10 for the different considered cuts in SIZE. The integral flux sensitivity after all cuts as a function of SIZE is shown in Table 3. Also shown is the γ-ray (excess events) rate measured for the Crab Nebula, that will be used as a reference to compute the γ-ray fluxes and/or limits from Cygnus X-1.

3.6 Spectrum unfolding

In order to produce our best estimate of the spectral shape of a given gamma-ray signal, we adopt the following simple and straight-forward procedure:

- Measure the number of excess events for each bin on estimated energy for the data:

$$N^{\text{data}}_{\text{excess},i} \tag{11}$$

  with i running over the number of estimated-energy bins.

- Measure the number of excess events for each bin on estimated energy for different MC samples with different spectral shapes:

$$N^{\text{MC},\alpha}_{\text{excess},i} \tag{12}$$

  with i running over the number of estimated-energy bins, and α over the different considered spectral shapes. In practice we will consider only power-law spectra and α can safely be associated to the photon index. The different spectral shapes are thus simulated by weighting the

Crab Nebula						
SIZE [phe]	$N_{\mathbf{on}}$ [events]	$N_{\mathbf{off}}$ [events]	N_{excess} [events]	**S** [SD]	**s** [% C.u.]	**R** [evnts/min]
200	596	548	486.4	27.4	2.91±0.01	2.22±0.11
300	516	336	448.6	28.8	2.47±0.01	2.05±0.10
400	439	242	390.4	27.8	2.41±0.01	1.78±0.10
600	343	134	316.0	26.6	2.22±0.01	1.44±0.08
800	282	93	263.2	24.9	2.23±0.01	1.20±0.08
1000	224	75	208.8	22.2	2.52±0.01	0.95±0.07
$E_{\mathbf{est}}$ [GeV]						
130	624	656	492.8	26.5	3.14±0.01	2.25±0.11
230	488	305	427.0	28.3	2.47±0.01	1.95±0.10
410	302	125	277.0	24.7	2.44±0.01	1.26±0.08
730	159	54	148.2	18.7	3.00±0.02	0.68±0.06
1300	50	15	47.0	10.7	4.98±0.11	0.21±0.03
2300	15	5	14.0	5.8	9.65±0.69	0.06±0.02

Table 3: From left to right: SIZE/Estimated-energy lower cut; number of events in the signal region; number of events in the background regions; number of excess events; statistical significance; integral flux sensitivity; and γ-ray rate obtained from Crab Nebula observations after all analysis cuts (see Equation 10). The total observation time is $T = 219.3$ minutes, and the number of areas used in background estimation $n = 5$.

events by:

$$\left(\frac{E_{\text{MC}}}{E_0}\right)^{-\alpha+\alpha_0} \tag{13}$$

where E_0 is an arbitrary normalization energy, α_0 the slope of the original MC sample and α the slope we want to simulate.

- Fit the MC histograms to the data histogram, letting α and the overall normalization free, and obtain the values of the parameters from such a fit.

4 Results

4.1 Search for gamma-ray signals

We perform a systematic search for γ-ray signals in Cygnus X-1 data sample. The search is carried out for the whole sample (sensitive to steady signals), orbital phase folded (sensitive to periodic signals) and on a night-by-night basis (sensitive to fast signals), following the prescriptions described in Section 3, and for lower SIZE cuts 200, 400 and 800 phe.

The results for the whole data sample are shown in table 4. The θ^2 distributions for the three considered lower SIZE cuts are shown in Figure 11. No positive signal is detected at 95% C.L. This allows us to impose very constraining upper limits to the γ-ray steady flux from Cygnus X-1, of the order of 1-2% of the Crab Nebula depending on the energy. These are, as far as we are aware of, the first limits established on this object at these energies. Note that these integral flux limits are

Cygnus X-1						
SIZE [phe]	N_{on} [events]	N_{off} [events]	N_{excess} [events]	**S** [SD]	**Eff.**	**Upp.** [evts (% CU)]
200	1063	5250	13.0 ± 35.7	0.4	0.91	94.1(1.8)
400	422	2090	4.0 ± 22.5	0.2	0.92	54.4(1.3)
800	175	843	6.4 ± 14.4	0.4	0.96	39.5(1.4)
E_{est} [GeV]						
130	1282	6344	13.2± 39.2	0.3	0.91	102.0(1.9)
230	585	2857	13.6± 26.4	0.5	0.92	73.9(1.6)
410	218	1070	4.0± 16.1	0.2	0.93	40.2(1.3)
730	96	449	6.2± 10.7	0.6	0.96	30.1(1.9)
1300	25	141	-3.2± 5.5	-0.6	0.99	9.0(1.8)
2300	8	45	-1.0± 3.1	-0.3	1.00	6.4(4.2)

Table 4: From left to right: SIZE/Estimated-energy lower cut, number of events in the signal region, number of events in the background regions, number of excess events, statistical significance of the excess, γ-ray detection efficiency and signal upper limit obtained from the whole Cygnus X-1 data sample. The total observation time is 2394.0 minutes. Upper limits are 95% confidence level and are quoted in number of events and in units of the γ-ray flux measured for the Crab nebula (Section 3.5).

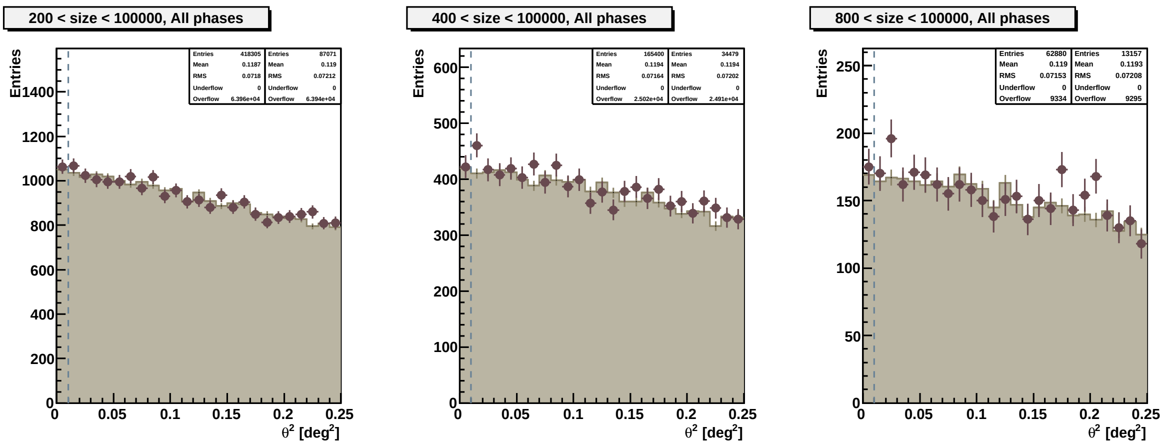

Figure 11: θ^2 distributions after HADRONNESS cut and for the different considered SIZE lower cuts, for the whole 2394.0 minutes of Cygnus X-1 observations. The vertical-dashed lines show the θ^2 cut.

computed assuming the same spectral shape as that of the Crab Nebula. The limits as a function of the (estimated) energy are shown in Figure 12 together with the Crab reference spectrum.

We search for periodic gamma-ray signals by phase-folding our data with the following orbital parameters: companion star inferior conjunction time (companion star between the black hole and observer) T_0 = 41163.029 (MJD) and orbital period P = 5.599829 days [1]. The results are shown in Table 5, for the three considered SIZE cuts and in Figure 13 for the cut SIZE>200 phe. A hint of signal at the 3.8 SD level is observed for the cut at 200 phe and in the phase bin [0.9,1.0], i.e. close to the companion star inferior conjunction. The corresponding significances for 400 and 800 phe SIZE cuts are 1.6 and 2.1 SD, respectively. The integrated observation time for this phase bin is 160.6 minutes. As will be shown below, out of them, 154.4 minutes (96.6%) correspond to the same

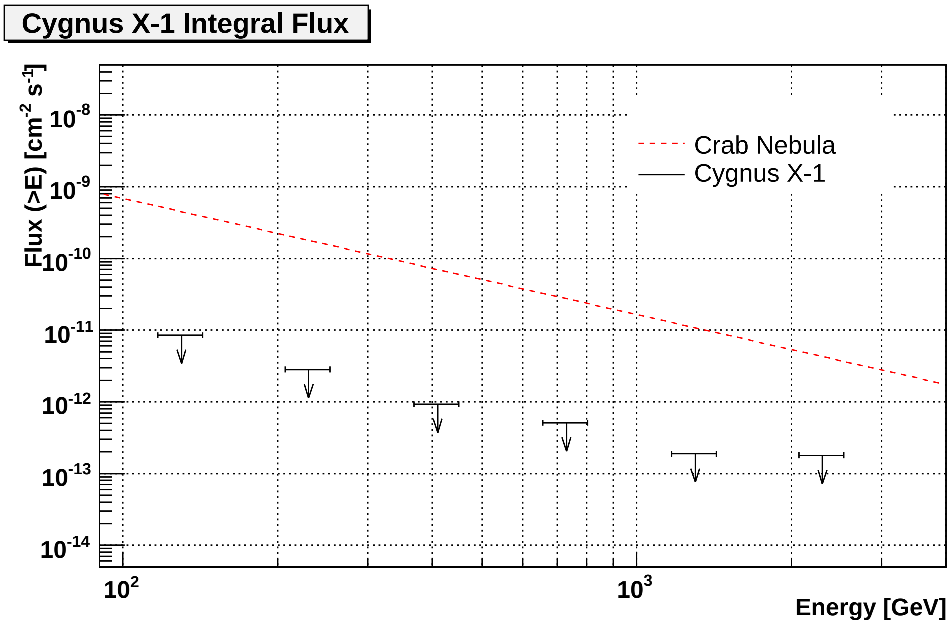

Figure 12: 95% CL limits to the integral flux of the steady gamma-ray emission from Cygnus X-1, as a function of the energy, assuming a 2.6 photon-index spectrum. The results correspond to the 2394.0 minutes of observations with MAGIC during cycle II.

observation night. Therefore, further discussion is left for the search of fast-variable signals.

Since Cygnus X-1 is expected to be a variable source we also look for gamma-ray signals for each observation night independently. The results are shown in Tables 6, 7 and 8. Since there are 26 good observation nights, the significance of the excesses are shown before and after correction for the number of trials (see Section 3.3).

A possible signal at 3.9 (3.0 post-trial) SD is found for MJD=54002.93 (observation night 25th September 2006) and SIZE>200 phe. The corresponding significances for SIZE>400 and SIZE>800 phe are 1.6 and 2.0 SD respectively. The total distribution of significances for all days and SIZE cuts is shown in Figure 14. Also shown are the signal confidence intervals for all observation nights. The θ^2 distributions and sky-maps for the different SIZE cuts and MJD=54002.93 are shown in Figure 15.

Following the procedure described in section 3.4 we split the sample corresponding to observation night 25/07/2006 (MJD=54002.88), whose forseen maximal significance for the cut SIZE>200 phe is 5.1 (4.5 post-trial) SD. The next highest-significance sample is that of night MJD=54006.94, for which we estimate a post-split maximal significance of 1.9 (0.3 post-trial) and therefore no split is performed. The results for the two new obtained samples are shown in Table 9. There is no evidence for significant detection in the first half-sample. However we obtain, for the second half-sample (referred to as 25/07/2006-B), a 4.8, 2.3 and 2.9 SD signal for SIZE lower cuts at 200, 400 and 800 phe. The θ^2 distributions and sky-maps for the different SIZE cuts are shown in Figure 17. This subsample is further subdivided since the maximal expected significance for SIZE>200 phe is 6.0 (5.4 post-trial) SD. The results of the second iteration are shown in table 10. In this case we obtain our signal almost equally distributed and therefore we stop our search for fast varying signals. The distribution of significances after the first iteration is shown in Figure 16.

All the different parameters characterizing the telescope's response during observation night 25/09/2006 have been carefully checked from the plots produced by the daily data check [16]. All the monitored

Cygnus X-1								
Phase	**T** [min]	$N_{\mathbf{on}}$ [evts]	$N_{\mathbf{off}}$ [evts]	$N_{\mathbf{excess}}$ [evts]	**S** [SD]	**Post** [SD]	ϵ	**Upp.** [evts (% CU)]
SIZE > 200 phe								
0.0-0.1	335.8	137	676	1.8± 12.8	0.1	0.0	0.93	30.72(4.1)
0.1-0.2	211.4	96	491	-2.2± 10.8	-0.2	0.0	0.95	21.44(4.6)
0.2-0.3	262.2	111	619	-12.8± 11.7	-1.1	0.0	0.95	11.81(2.0)
0.3-0.4	188.7	72	453	-18.6± 9.5	-1.9	0.7	0.88	1.23(0.3)
0.4-0.5	307.9	139	687	1.6± 12.9	0.1	0.0	0.95	29.94(4.4)
0.5-0.6	307.3	143	647	13.6± 13.0	1.1	0.0	0.91	45.35(6.7)
0.6-0.7	127.1	49	277	-6.4± 7.8	-0.8	0.0	0.92	10.83(3.8)
0.7-0.8	54.0	28	117	4.6± 5.7	0.8	0.0	0.94	18.48(15.4)
0.8-0.9	439.1	192	983	-4.6± 15.2	-0.3	0.0	0.90	29.61(3.0)
0.9-1.0	160.4	96	303	35.4± 10.4	3.8	3.1	0.90	66.12(18.6)
SIZE > 400 phe								
0.0-0.1	335.8	59	275	4.0± 8.4	0.5	0.0	0.94	23.41(3.9)
0.1-0.2	211.4	36	189	-1.8± 6.6	-0.3	0.0	0.96	13.00(3.5)
0.2-0.3	262.2	44	238	-3.6± 7.3	-0.5	0.0	0.96	12.56(2.7)
0.3-0.4	188.7	32	172	-2.4± 6.2	-0.4	0.0	0.89	12.45(3.7)
0.4-0.5	307.9	56	283	-0.6± 8.2	-0.1	0.0	0.97	17.47(3.2)
0.5-0.6	307.3	52	245	3.0± 7.9	0.4	0.0	0.93	21.55(3.9)
0.6-0.7	127.1	19	116	-4.2± 4.9	-0.8	0.0	0.94	6.90(3.0)
0.7-0.8	54.0	10	40	2.0± 3.4	0.6	0.0	0.96	10.56(11.0)
0.8-0.9	439.1	78	403	-2.6± 9.7	-0.3	0.0	0.92	19.32(2.5)
0.9-1.0	160.4	36	132	9.6± 6.4	1.6	0.4	0.92	26.11(9.1)
SIZE > 800 phe								
0.0-0.1	335.8	22	114	-0.8± 5.2	-0.2	0.0	0.96	11.06(2.7)
0.1-0.2	211.4	12	75	-3.0± 3.9	-0.7	0.0	0.98	5.91(2.3)
0.2-0.3	262.2	16	99	-3.8± 4.5	-0.8	0.0	0.97	6.33(2.0)
0.3-0.4	188.7	16	63	3.4± 4.3	0.8	0.0	0.93	14.38(6.3)
0.4-0.5	307.9	21	110	-1.0± 5.0	-0.2	0.0	0.98	10.40(2.8)
0.5-0.6	307.3	24	95	5.0± 5.3	1.0	0.0	0.95	17.91(4.9)
0.6-0.7	127.1	8	50	-2.0± 3.2	-0.6	0.0	0.94	5.78(3.8)
0.7-0.8	54.0	7	22	2.6± 2.8	1.0	0.0	0.97	9.87(15.2)
0.8-0.9	439.1	31	168	-2.6± 6.1	-0.4	0.0	0.95	11.25(2.1)
0.9-1.0	160.4	18	49	8.2± 4.5	2.1	1.0	0.94	19.95(10.4)

Table 5: From left to right: orbital phase, observation time, number of events in the signal region, number of events in the background regions, number of excess events, statistical significance of the excess, post-trial equivalent significance, mean γ-ray detection efficiency and signal upper limit for Cygnus X-1. Upper limits are 95% confidence level and are quoted in number of events and in units of the γ-ray flux measured for the Crab Nebula (Section 3.5).

parameters, e.g. the camera HV, LV, temperature and humidity; the discriminator thresholds, time delays and trigger rates; the external temperature and humidity; the measured mispointing; the calibration constants, etc are well within the nominal values. The results for the two wobble positions analyzed independently are statistically compatible at the 3% level. Also, the results presented in this section have been cross-checked and confirmed by at least two independent data analyses [14, 15].

Cygnus X-1, SIZE > 200 phe								
MJD [days]	**T** [min]	N_{on} [evts]	N_{off} [evts]	N_{excess} [evts]	**S** [SD]	**Post** [SD]	ϵ	**Upp.** [evts (% CU)]
53942.05	61.1	20	82	3.6± 4.8	0.8	0.0	0.97	15.02(11.1)
53964.89	105.6	41	181	4.8± 6.9	0.7	0.0	0.93	21.49(9.2)
53965.89	195.3	83	481	-13.2± 10.1	-1.3	0.0	0.89	8.74(2.0)
53966.93	124.8	76	333	9.4± 9.5	1.0	0.0	0.90	33.07(11.9)
53967.99	48.5	17	130	-9.0± 4.7	-1.7	0.1	0.84	1.57(1.5)
53968.88	237.5	112	582	-4.4± 11.6	-0.4	0.0	0.87	22.76(4.3)
53994.95	53.6	19	115	-4.0± 4.9	-0.8	0.0	0.98	6.84(5.8)
53995.96	58.1	17	99	-2.8± 4.6	-0.6	0.0	0.95	7.76(6.0)
53996.86	176.2	69	337	1.6± 9.1	0.2	0.0	0.95	22.15(5.7)
53997.88	132.7	49	219	5.2± 7.6	0.7	0.0	0.95	22.95(7.8)
54000.85	165.2	81	348	11.4± 9.7	1.2	0.0	0.92	35.41(9.7)
54002.88	154.4	97	301	36.8± 10.4	3.9	3.0	0.91	67.85(19.8)
54003.86	166.9	68	375	-7.0± 9.1	-0.8	0.0	0.91	13.35(3.6)
54004.89	123.3	51	285	-6.0± 7.9	-0.7	0.0	0.94	11.33(4.1)
54005.91	87.9	33	176	-2.2± 6.3	-0.3	0.0	0.97	11.88(6.1)
54006.94	28.0	15	48	5.4± 4.1	1.4	0.0	0.99	15.26(24.6)
54020.89	65.5	28	183	-8.6± 5.9	-1.4	0.0	0.97	4.27(2.9)
54021.89	68.6	26	161	-6.2± 5.7	-1.0	0.0	0.97	6.30(4.1)
54022.89	58.1	29	137	1.6± 5.9	0.3	0.0	1.00	14.55(11.3)
54028.86	68.6	30	133	3.4± 5.9	0.6	0.0	0.91	18.28(12.0)
54029.89	33.5	22	93	3.4± 5.1	0.7	0.0	0.93	15.93(21.5)
54030.86	19.6	7	44	-1.8± 3.0	-0.6	0.0	0.96	5.41(12.5)
54048.82	47.2	27	127	1.6± 5.7	0.3	0.0	0.94	14.99(14.3)
54049.82	47.9	23	145	-6.0± 5.4	-1.1	0.0	0.93	6.09(5.7)
54056.82	27.1	11	81	-5.2± 3.8	-1.3	0.0	0.94	3.55(5.9)
54057.82	21.5	6	24	1.2± 2.6	0.5	0.0	0.97	7.96(16.7)

Table 6: From left to right: Modified Julian Date, observation time, number of events in the signal region, number of events in the background regions, number of excess events, statistical significance of the excess, post-trial equivalent significance, mean γ-ray detection efficiency and signal upper limit for a cut SIZE>200 phe and the different observation nights of Cygnus X-1. Upper limits are 95% confidence level and are quoted in number of events and in units of the γ-ray flux measured for the Crab Nebula (Section 3.5).

Cygnus X-1, SIZE > 400 phe								
MJD [days]	**T** [min]	N_{on} [evts]	N_{off} [evts]	N_{excess} [evts]	**S** [SD]	**Post** [SD]	ϵ	**Upp.** [evts (% CU)]
53942.05	61.1	10	34	3.2± 3.4	1.0	0.0	0.97	11.59(10.7)
53964.89	105.6	14	84	-2.8± 4.2	-0.6	0.0	0.95	6.95(3.7)
53965.89	195.3	36	178	0.4± 6.6	0.1	0.0	0.90	16.31(4.7)
53966.93	124.8	29	133	2.4± 5.9	0.4	0.0	0.92	16.73(7.5)
53967.99	48.5	5	52	-5.4± 2.7	-1.7	0.1	0.86	1.04(1.2)
53968.88	237.5	43	232	-3.4± 7.2	-0.5	0.0	0.89	13.54(3.2)
53994.95	53.6	9	62	-3.4± 3.4	-0.9	0.0	0.98	4.50(4.7)
53995.96	58.1	8	45	-1.0± 3.1	-0.3	0.0	0.96	6.64(6.4)
53996.86	176.2	29	143	0.4± 5.9	0.1	0.0	0.96	13.92(4.4)
53997.88	132.7	19	96	-0.2± 4.8	-0.0	0.0	0.96	10.92(4.6)
54000.85	165.2	26	133	-0.6± 5.6	-0.1	0.0	0.94	12.48(4.2)
54002.88	154.4	36	132	9.6± 6.4	1.6	0.1	0.92	26.10(9.5)
54003.86	166.9	30	145	1.0± 6.0	0.2	0.0	0.92	15.43(5.2)
54004.89	123.3	22	107	0.6± 5.1	0.1	0.0	0.95	12.67(5.8)
54005.91	87.9	14	76	-1.2± 4.1	-0.3	0.0	0.97	8.41(5.4)
54006.94	28.0	6	19	2.2± 2.6	0.9	0.0	0.99	8.82(17.7)
54020.89	65.5	12	66	-1.2± 3.8	-0.3	0.0	0.98	7.75(6.6)
54021.89	68.6	11	61	-1.2± 3.7	-0.3	0.0	0.98	7.39(6.0)
54022.89	58.1	14	46	4.8± 4.0	1.3	0.0	1.00	14.20(13.7)
54028.86	68.6	11	52	0.6± 3.6	0.2	0.0	0.93	9.73(8.0)
54029.89	33.5	10	40	2.0± 3.4	0.6	0.0	0.96	10.56(17.7)
54030.86	19.6	3	16	-0.2± 1.9	-0.1	0.0	0.96	5.05(14.5)
54048.82	47.2	10	39	2.2± 3.4	0.7	0.0	0.95	10.81(12.8)
54049.82	47.9	7	64	-5.8± 3.1	-1.6	0.1	0.94	1.43(1.7)
54056.82	27.1	4	21	-0.2± 2.2	-0.1	0.0	0.95	5.70(11.8)
54057.82	21.5	0	0	0.0± 0.0	0.0	0.0	1.00	—

Table 7: From left to right: Modified Julian Date, observation time, number of events in the signal region, number of events in the background regions, number of excess events, statistical significance of the excess, post-trial equivalent significance, mean γ-ray detection efficiency and signal upper limit for a cut SIZE>400 phe and the different observation nights of Cygnus X-1. Upper limits are 95% confidence level and are quoted in number of events and in units of the γ-ray flux measured for the Crab Nebula (Section 3.5).

Cygnus X-1, SIZE > 800 phe								
MJD [days]	**T** [min]	$N_{\mathbf{on}}$ [evts]	$N_{\mathbf{off}}$ [evts]	$N_{\mathbf{excess}}$ [evts]	**S** [SD]	**Post** [SD]	ϵ	**Upp.** [evts (% CU)]
53942.05	61.1	3	14	0.2± 1.9	0.1	0.0	0.99	5.30(7.2)
53964.89	105.6	3	32	-3.4± 2.1	-1.4	0.0	0.97	1.83(1.4)
53965.89	195.3	15	67	1.6± 4.2	0.4	0.0	0.92	12.17(5.2)
53966.93	124.8	10	53	-0.6± 3.5	-0.2	0.0	0.94	7.97(5.3)
53967.99	48.5	3	18	-0.6± 1.9	-0.3	0.0	0.86	5.17(8.9)
53968.88	237.5	16	102	-4.4± 4.5	-0.9	0.0	0.94	5.91(2.1)
53994.95	53.6	3	24	-1.8± 2.0	-0.8	0.0	1.00	3.32(5.2)
53995.96	58.1	3	21	-1.2± 2.0	-0.6	0.0	0.97	4.00(5.7)
53996.86	176.2	13	56	1.8± 3.9	0.5	0.0	0.96	11.27(5.3)
53997.88	132.7	11	43	2.4± 3.6	0.7	0.0	0.97	11.15(7.0)
54000.85	165.2	11	46	1.8± 3.6	0.5	0.0	0.94	10.84(5.5)
54002.88	154.4	18	50	8.0± 4.5	2.0	0.4	0.94	19.72(10.6)
54003.86	166.9	8	57	-3.4± 3.2	-1.0	0.0	0.93	4.34(2.2)
54004.89	123.3	7	42	-1.4± 2.9	-0.5	0.0	0.97	5.80(3.9)
54005.91	87.9	7	31	0.8± 2.9	0.3	0.0	0.98	7.91(7.5)
54006.94	28.0	2	11	-0.2± 1.6	-0.1	0.0	0.99	—)
54020.89	65.5	5	31	-1.2± 2.5	-0.5	0.0	0.99	5.01(6.4)
54021.89	68.6	7	24	2.2± 2.8	0.8	0.0	0.98	9.32(11.3)
54022.89	58.1	5	17	1.6± 2.4	0.7	0.0	1.00	7.72(11.1)
54028.86	68.6	5	23	0.4± 2.4	0.2	0.0	0.96	6.79(8.2)
54029.89	33.5	7	22	2.6± 2.8	1.0	0.0	0.97	9.87(24.6)
54030.86	19.6	0	6	-1.2± 0.5	0.0	0.0	1.00	—
54048.82	47.2	4	12	1.6± 2.1	0.8	0.0	0.97	7.36(13.0)
54049.82	47.9	3	29	-2.8± 2.0	-1.2	0.0	0.96	2.46(4.3)
54056.82	27.1	3	8	1.4± 1.8	0.9	0.0	0.96	6.67(20.5)
54057.82	21.5	0	0	0.0± 0.0	0.0	0.0	1.00	—

Table 8: From left to right: Modified Julian Date, observation time, number of events in the signal region, number of events in the background regions, number of excess events, statistical significance of the excess, post-trial equivalent significance, mean γ-ray detection efficiency and signal upper limit for a cut SIZE>800 phe and the different observation nights of Cygnus X-1. Upper limits are 95% confidence level and are quoted in number of events and in units of the γ-ray flux measured for the Crab Nebula (Section 3.5).

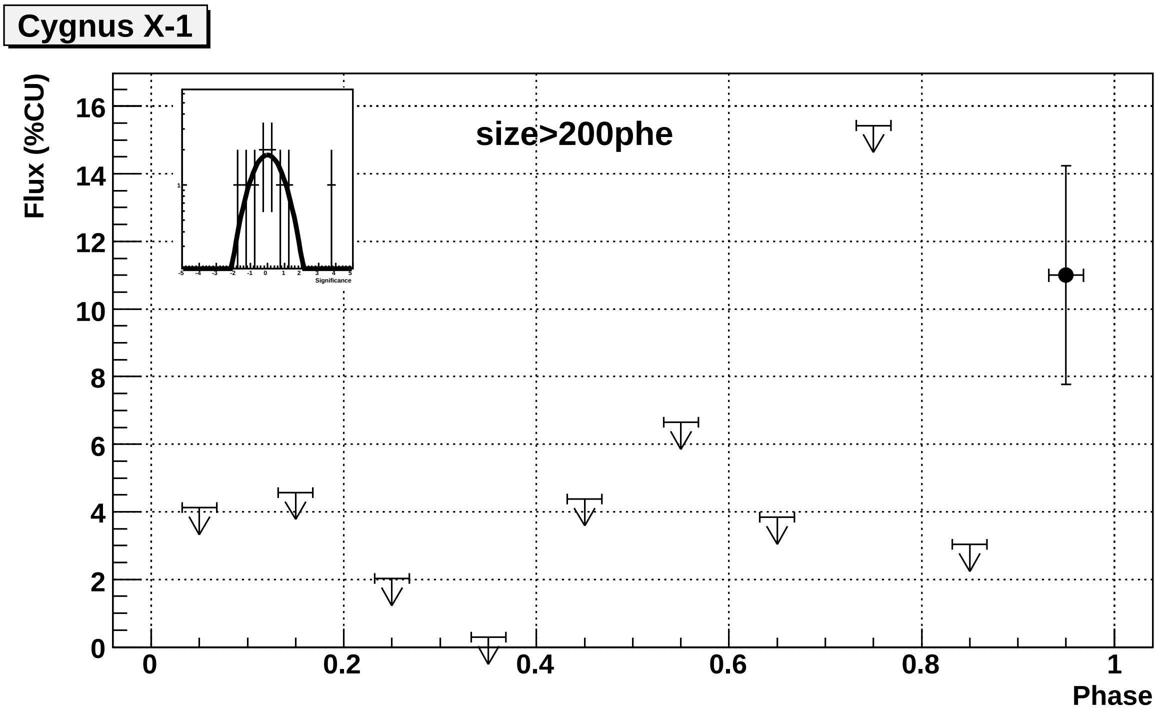

Figure 13: Integral flux for a cut on SIZE>200 phe as a function of the orbital phase for Cygnus X-1. Upper limits are at 95% (∼ 2 SD) CL 95% (∼ 2 SD) and assume a Crab-like spectral shape. Two sided intervals are at 1 SD. The inset shows the distribution of significances (before trial correction and in SD) together with a fit to a zero-mean, unity-sigma Gaussian distribution.

Cygnus X-1, 25/09/2006							
MJD [days]	**T** [min]	N_{on} [evts]	N_{off} [evts]	N_{excess} [evts]	**S** [SD]	**Post** [SD]	ϵ
SIZE > 200 phe							
54002.88	75.5	33	150	3.0± 6.2	0.5	0.0	0.93
54002.93	78.9	64	151	33.8± 8.4	4.8	4.0	0.89
SIZE > 400 phe							
54002.88	75.5	12	64	-0.8± 3.8	-0.2	-0.0	0.94
54002.93	78.9	24	68	10.4± 5.2	2.3	0.7	0.92
SIZE > 800 phe							
54002.88	75.5	4	25	-1.0± 2.2	-0.4	-0.0	0.96
54002.93	78.9	14	25	9.0± 3.9	2.9	1.7	0.94

Table 9: From left to right: Modified Julian Date, observation time, number of events in the signal region, number of events in the background regions, number of excess events, statistical significance of the excess, post-trial equivalent significance, mean γ-ray detection efficiency and signal upper limit for Cygnus X-1 observation night 25/09/2006.

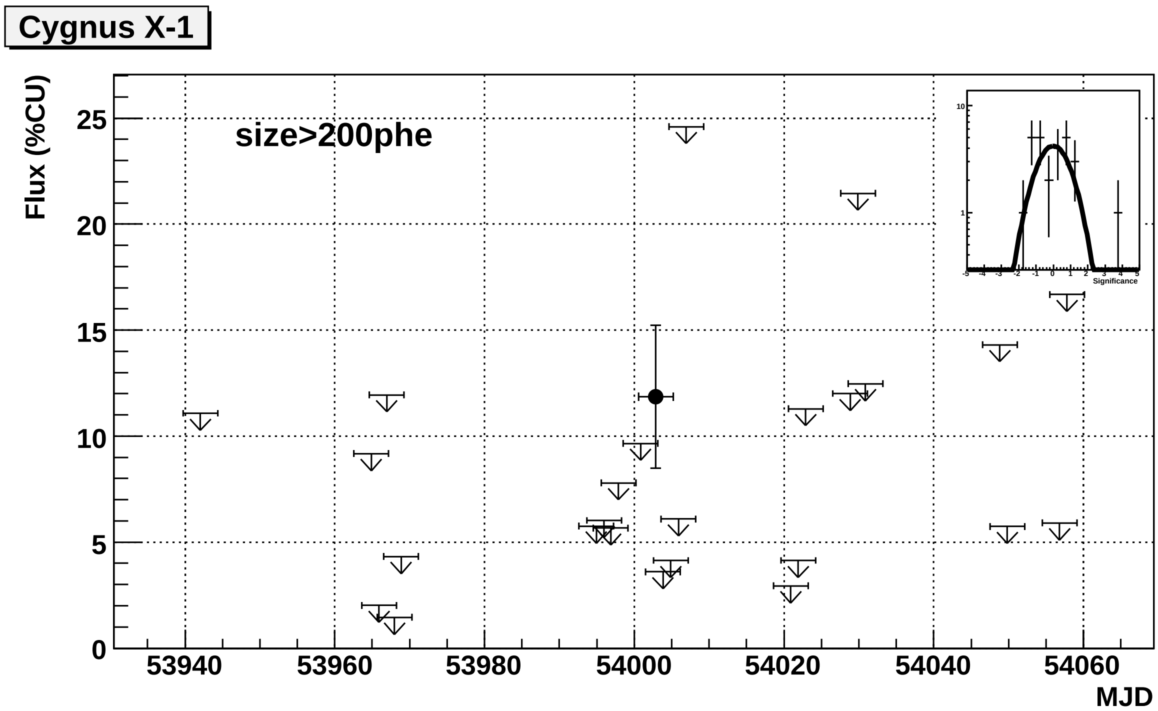

Figure 14: Integral flux for a cut on SIZE>200 phe as a function of the time for Cygnus X-1. Upper limits are at 95% ($\sim$ 2 SD) CL and assume a Crab-like spectral shape. Two sided intervals are at 1 SD. The inset shows the distribution of significances (before trial correction and in SD) together with a fit to a zero-mean, unity-sigma Gaussian distribution.

Cygnus X-1, 25/09/2006-B							
MJD [days]	**T** [min]	$N_{\mathbf{on}}$ [evts]	$N_{\mathbf{off}}$ [evts]	$N_{\mathbf{excess}}$ [evts]	**S** [SD]	**Post** [SD]	ϵ
SIZE > 200 phe							
54002.93	38.9	30	71	15.8± 5.7	3.2	2.1	0.90
54002.96	40.0	34	80	18.0± 6.1	3.5	2.5	0.88
SIZE > 400 phe							
54002.93	38.9	12	35	5.0± 3.7	1.5	0.0	0.93
54002.96	40.0	12	33	5.4± 3.6	1.7	0.1	0.91
SIZE > 800 phe							
54002.93	38.9	7	10	5.0± 2.7	2.4	0.9	0.95
54002.96	40.0	7	15	4.0± 2.8	1.7	0.1	0.92

Table 10: From left to right: Modified Julian Date, observation time, number of events in the signal region, number of events in the background regions, number of excess events, statistical significance of the excess, post-trial equivalent significance, mean γ-ray detection efficiency and signal upper limit for Cygnus X-1 observation sample 25/09/2006-B.

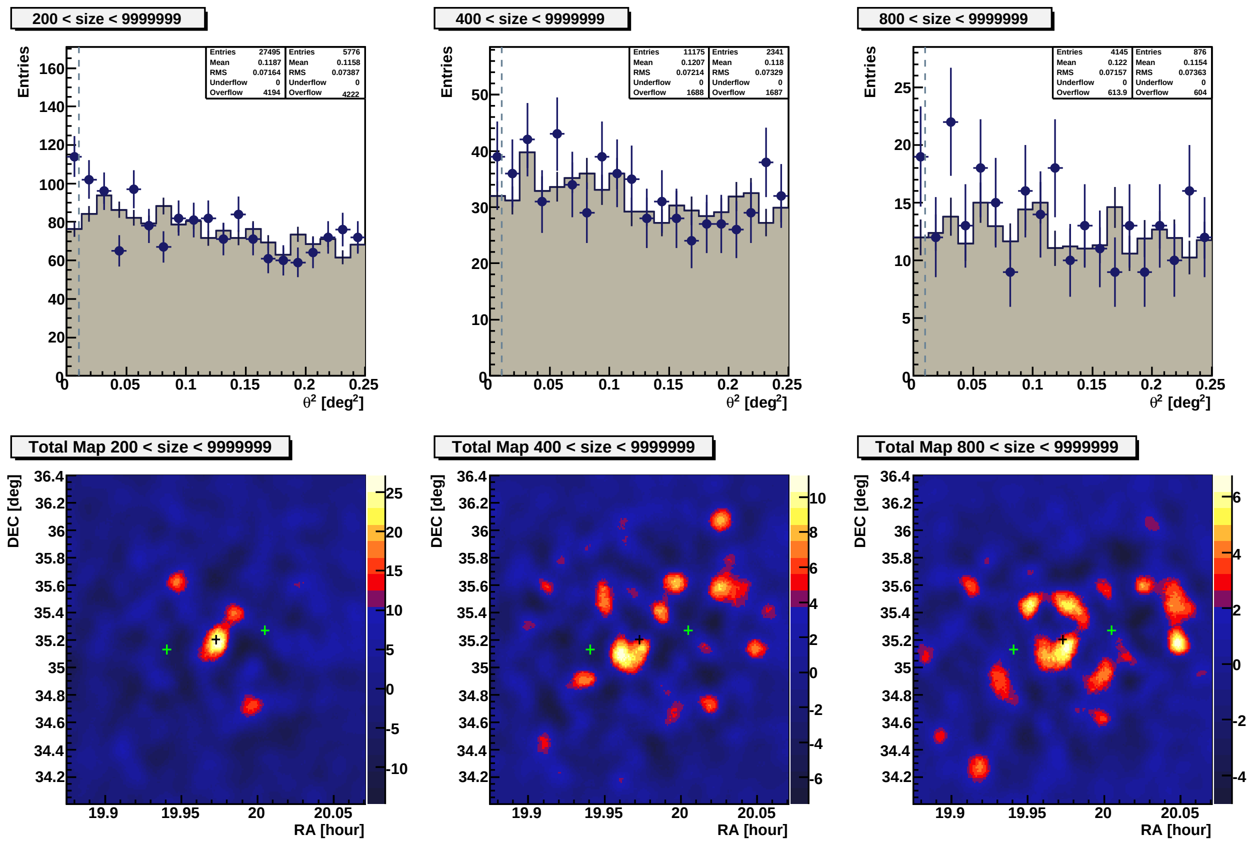

Figure 15: Observation night 25th September 2006 (MJD=54002.88). Top: θ^2 distributions after HADRONNESS cut and for the different considered SIZE lower cuts; the vertical-dashed lines show the θ^2 cut. Bottom: Maps of excess events around the position of Cygnus X-1 (marked with a black cross) after HADRONNESS cut and the different considered SIZE lower cuts; the light-green crosses show the the telescope's pointing positions.

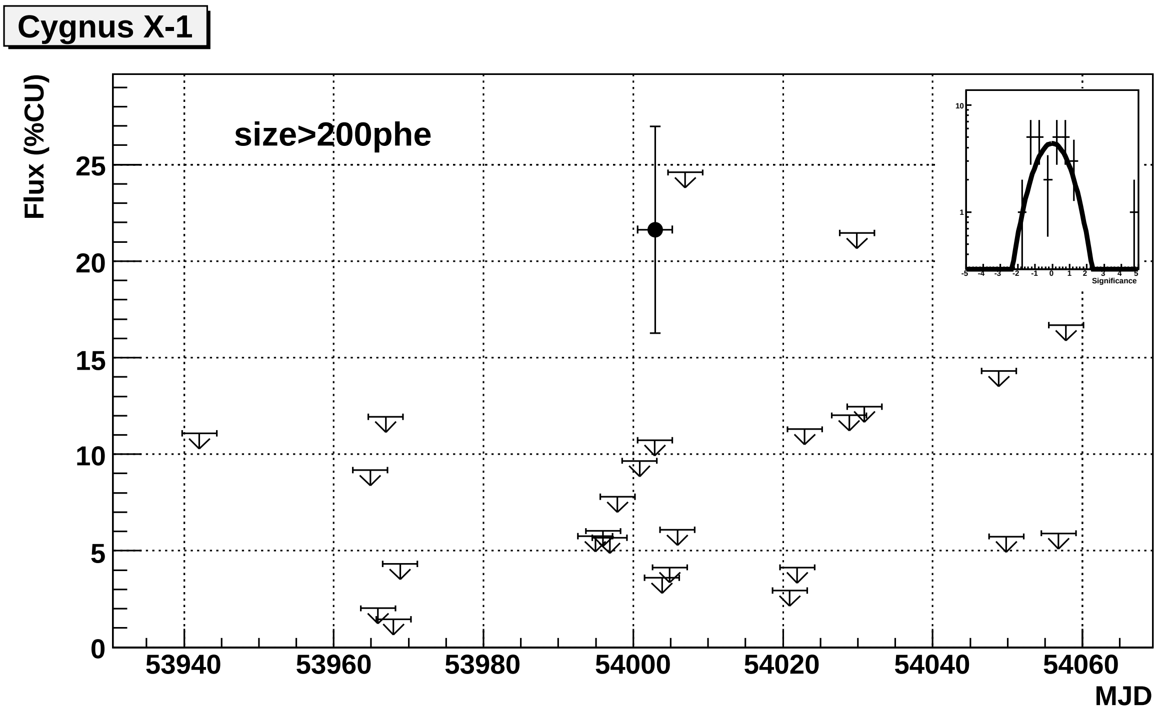

Figure 16: Integral flux for a cut on SIZE>200 phe as a function of the time for Cygnus X-1 after splitting sample 25/09/2006. Upper limits are at 95% ($\sim$ 2 SD) CL and assume a Crab-like spectral shape. Two sided intervals are at 1 SD. The inset shows the distribution of significances (before trial correction and in SD) together with a fit to a zero-mean, unity-sigma Gaussian distribution.

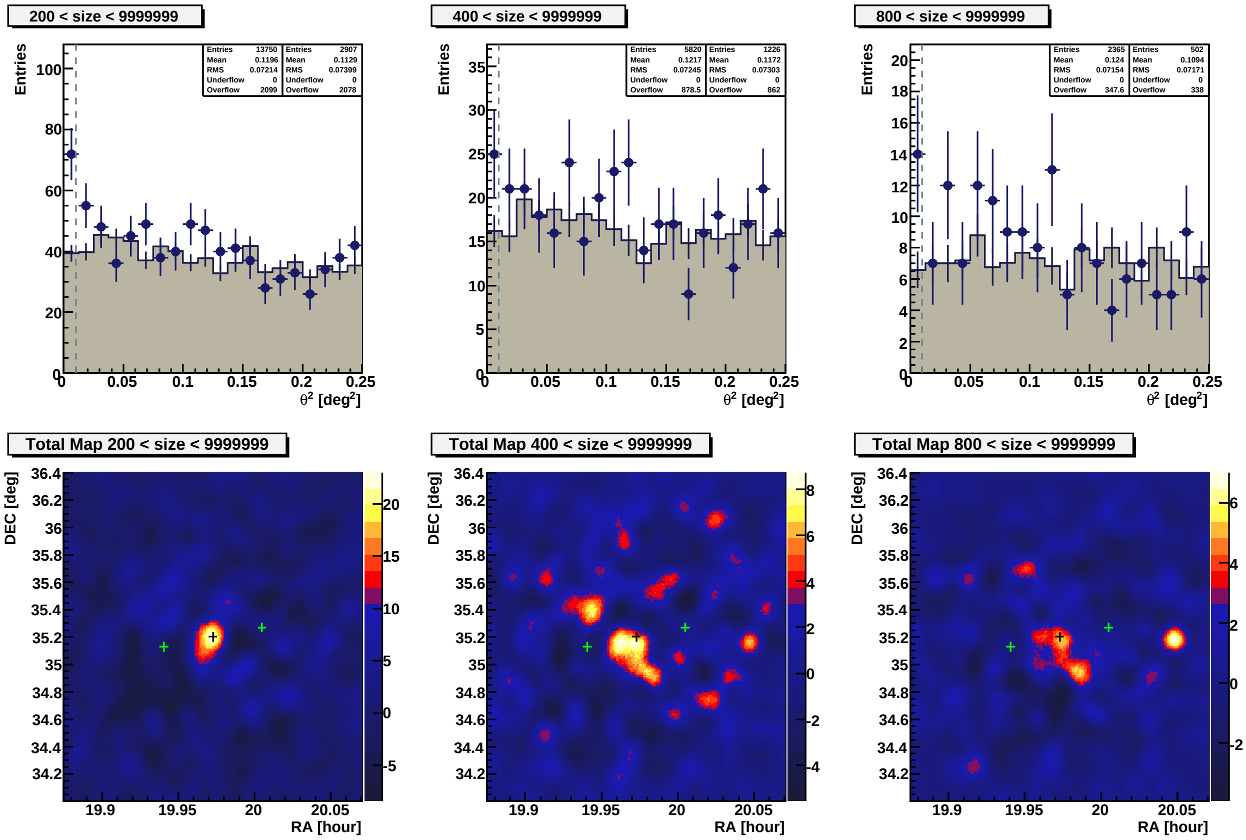

Figure 17: Observation night 25th September 2006 sample B (MJD=54002.93). Top: θ^2 distributions after HADRONNESS cut and for the different considered SIZE lower cuts; the vertical-dashed lines show the θ^2 cut. Bottom: Maps of excess events around the position of Cygnus X-1 (marked with a black cross) after HADRONNESS cut and the different considered SIZE lower cuts; the light-green crosses show the the telescope's pointing positions.

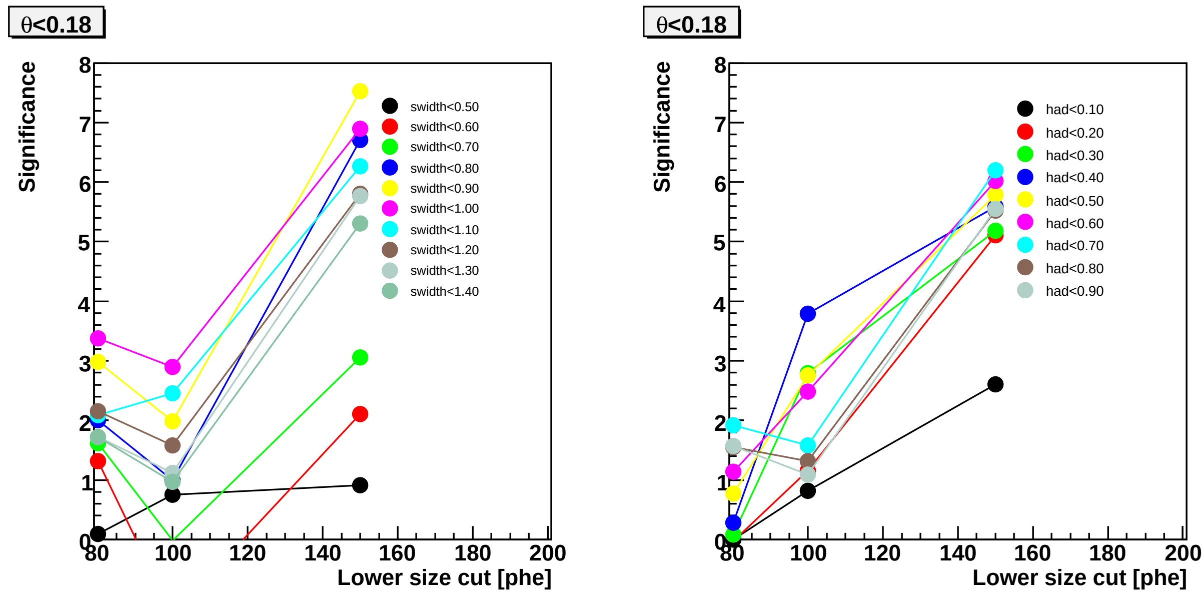

Figure 18: Significance obtained from 219.3 minutes of observations of the Crab nebula, as a function of the cut on sWIDTH (left) and HADRONNESS (right), for the SIZE bins [80-100], [100-150] and [150-200] phe and a cut on $\theta < 0.18°$.

4.2 Trying to increase the signal significance

We have tried to increase the significance of the detection shown in Section 4.1 in an unbiased way. First, we have tried to include lower SIZE bins. Using the Crab nebula sample described in Section 2, we study the significance as a function of the upper cut on HADRONNESS and on scaled WIDTH (sWIDTH) for three SIZE bins, namely [80-100], [100-150] and [150-200] phe. The results are shown in Figure 18. Figure 19 shows the θ^2 distributions and sky-maps for the three considered SIZE bins and a cut on sWIDTH<1, for which the obtained significances are 3.4, 2.9 and 7.0 SD, respectively. As shown in the sky-maps, there is a sizeable asymmetry in the distribution of excesses attributable to the camera acceptance inhomogeneity. The intensity of the excess seen at the source position for the lower SIZE bins are of the same order or lower than the asymetry amplitude and cannot therefore be considered as physical. The same conclusions can be drawn when applying a cut on HADRONNESS. We conclude that, at least with this analysis, we have no sensitivity below 150 phe.

For the bin 150<SIZE<200 phe and cuts sWIDTH<1.0 and $\theta < 0.18°$ we obtain 17% Crab flux sensitivity. The results for Cygnus X-1 for this SIZE bin and sWIDTH<1.0 are shown in Figure 20. No signal is detected.

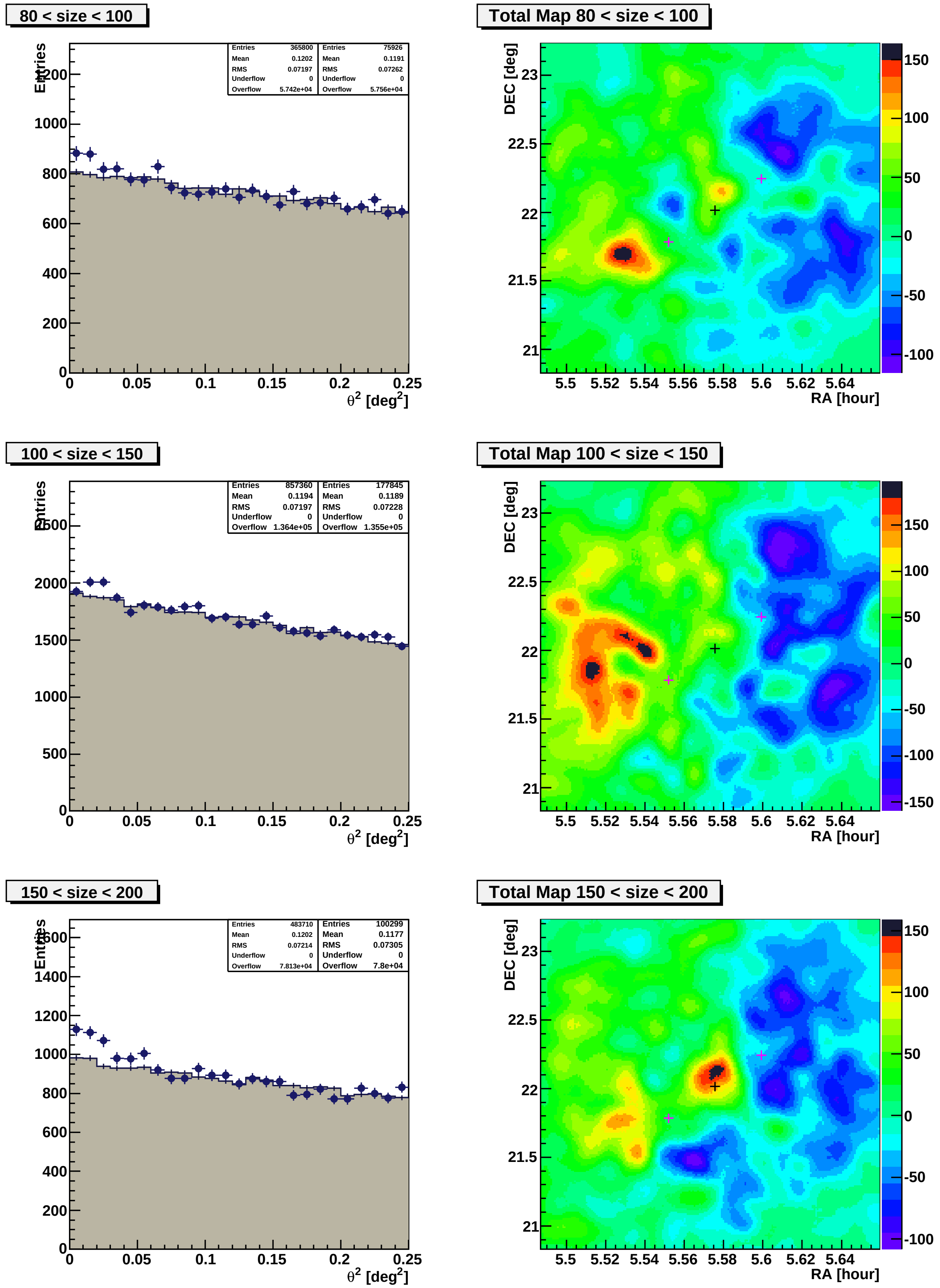

Figure 19: θ^2 distributions (left) and sky maps for (right) for the Crab nebula observations, for three SIZE bins and a cut on sWIDTH<1.

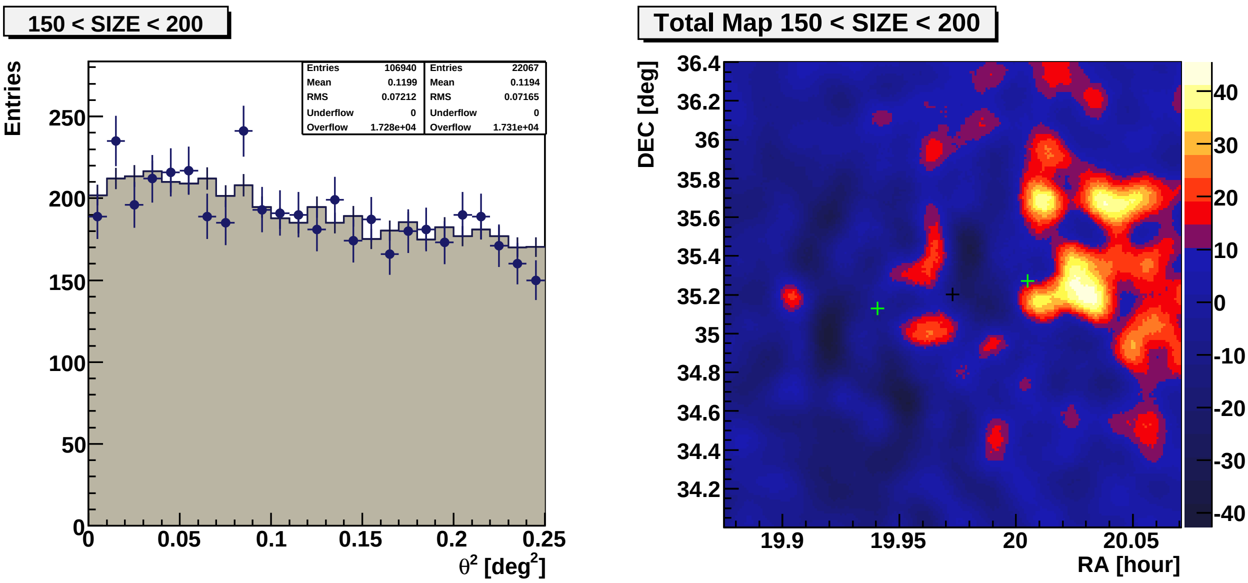

Figure 20: θ^2 distributions (left) and sky maps (right) for Cygnus X-1 sample 25/09/2006-B, for 150<SIZE<200 phe and sWIDTH<1.

A second attempt to increase the significance is carried out by increasing the sample used to estimate the number of background events in the signal region. With our background estimation method (described in section 3.2) we automatically have 5 times more background statistics than signal. By assuming 10 times more background statistics and the number of ON and OFF events quoted in Table 9 we expect a significance of 5.0 SD. For a infinitely well known background the significance tends to 5.3 SD. To increase the OFF sample, we use the background estimation samples corresponding to other observation nights. All data taken at zenith angles between 18 and 36° (as for sample 25/09/2006-B) and with rate values deviating less than 10% from those for sample 25/09/2006-B are used (see Figure 21). The selected sample corresponds to an observation time of 264.9 minutes, that is, the ratio OFF/ON is ~ 22. The number of OFF events in the signal region is 688, yielding a significance of 4.9 SD. The corresponding θ^2 distribution and sky-map are shown in Figure 22.

The computation of the post-trial significance for the subsample 25/09/2006-B (see Table 9) is somewhat biased, since we have selected *a posteriori* to split the sample with maximal significance. In order to compute the real post-trial significance we have to consider the following two independent probabilities: P_1: the probability of obtaining a given significance for sample 25/09/2006 (before splitting), taking into the number of trials; and P_2: the probability that the signal is concentrated in one half of the data sample. P_1 is shown in Table 6 and is equivalent to 3.0 SD. We have increased the OFF statistics for this sample as described above, and obtained $N_{\rm on} = 97$, $N_{\rm off} = 1419$ and a ratio OFF/ON ~ 23, with a probability after 26 trials of 8.04×10^{-4} (3.2 SD). To compute P_2 we have made a toy MC simulation. We have generated arrival times for the $N_{\rm on}$ and the $N_{\rm off}$ surviving events in sample and checked how many times we get 4.9 SD or higher in one of the considered half-samples, obtaining $P_2 = 3.6 \times 10^{-3}$. The total probability is the given by $P_1 \times P_2 = 2.89 \times 10^{-6}$, equivalent to 4.5 SD.

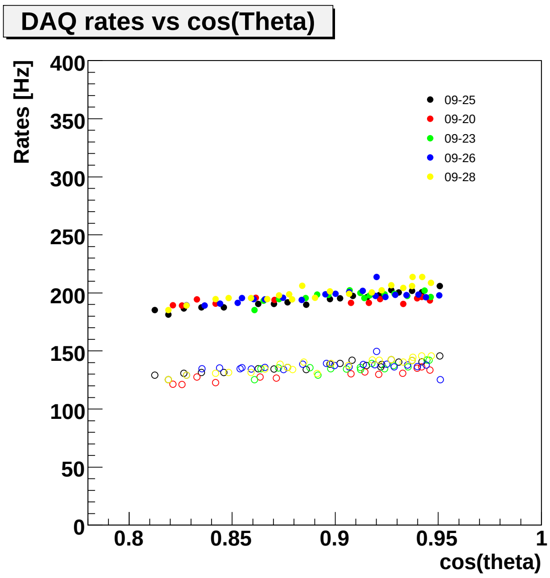

Figure 21: Event rate before (solid) and after (empty) image cleaning as a function of the zenith angle for the samples used for background estimation for sample 25/09/2006-B.

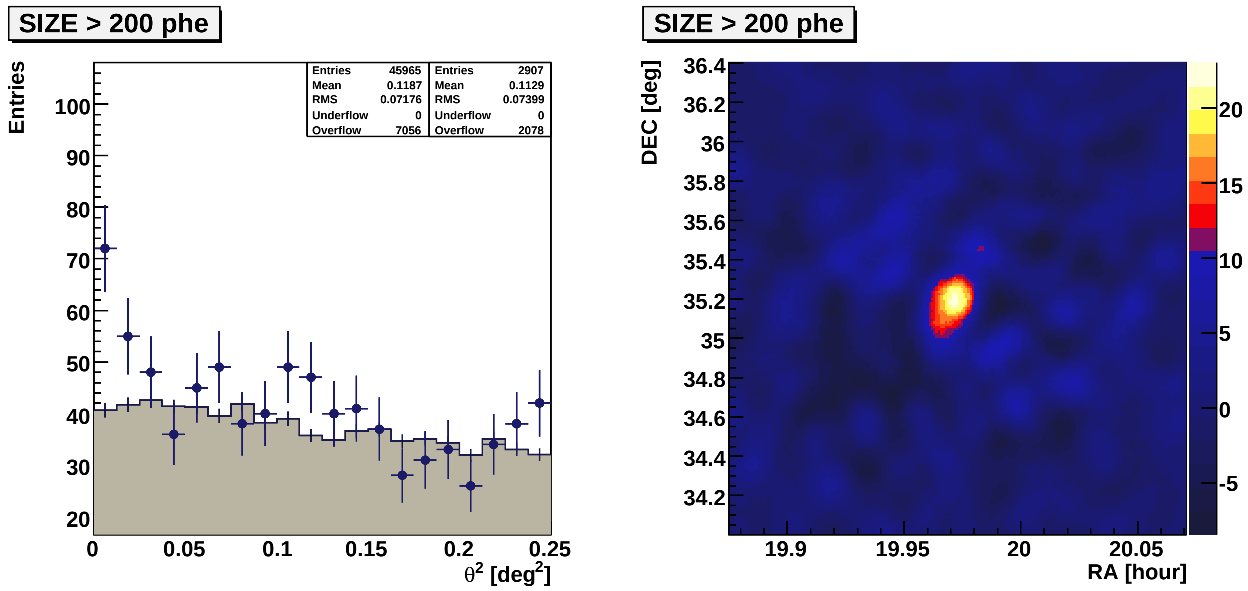

Figure 22: θ^2 distributions (left) and sky maps for (right) for Cygnus X-1 sample 25/09/2006-B for SIZE>200 phe using $\sim$ 22 times more OFF than ON statistics.

4.3 Spectrum, source position and extension

We have computed the spectrum corresponding to sample 25/09/2006-B. For this we use the procedure described in Section 3.6, using the corrections by the increased DT effect [9, 10]. The results are shown in Table 11 and Figure 23. The obtained spectrum is well fitted by a power-law function:

$$\frac{dN}{dA\ dt\ dE} = (2.3 \pm 0.6) \times 10^{-12} (E/1\ \mathrm{TeV})^{-3.2\pm0.6} \quad \mathrm{cm}^{-2}\mathrm{s}^{-1}\mathrm{TeV}^{-1} \tag{14}$$

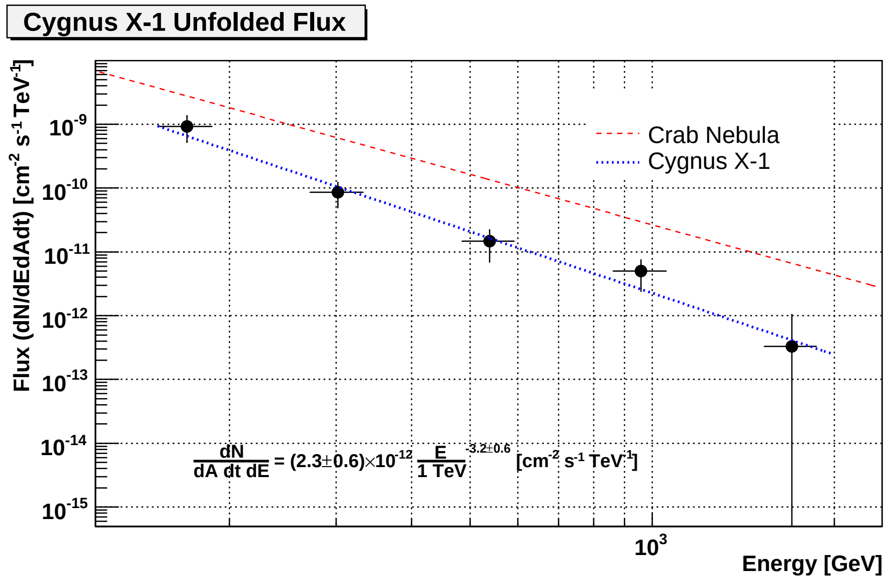

Figure 23: Differential spectrum of Cygnus X-1 corresponding to 78.9 minutes of observations started on MJD=54002.93 (sample 25/09/2006-B).

Cygnus X-1 25/09/2006-B						
$E_{\mathbf{est}}$ [GeV]	$N_{\mathbf{on}}$ [events]	$N_{\mathbf{off}}$ [events]	N_{excess} [events]	**S** [SD]	ϵ	**R** [evnts/min]
130-230	30	104	9.2± 5.8	1.7	0.88	0.13± 0.08
230-410	26	67	12.6± 5.4	2.7	0.88	0.18± 0.08
410-730	8	13	5.4± 2.9	2.3	0.90	0.08± 0.04
730-1300	7	10	5.0± 2.7	2.4	0.95	0.07± 0.03
1300-2300	2	7	0.6± 1.5	0.4	0.96	0.01± 0.02

Table 11: From left to right: Estimated-energy bin; number of events in the signal region; number of events in the background regions; number of excess events; statistical significance; mean γ-ray detection efficiency; and γ-ray rate for Cygnus X-1 25/09/2007-B sample. The total observation time is $T = 78.9$ minutes, and the number of areas used in background estimation $n = 5$.

where the quoted errors are statistical only.

In order to determine the source position we project into the RA axis a band of DEC $=$ DEC$_0 \pm 0.1°$ and into DEC a band of RA $=$ RA$_0 \pm 0.008$ hours. The source RA and DEC coordinates are computed from the Gaussian fit to the central part of the obtained 1-D projections (See Figure 24 left plots). This yields the following result: $\alpha = 19^{\text{h}}58^{\text{m}}17^{\text{s}}$, $\delta = 35°12''8'$. The statistical error is estimated as $\Delta/\sqrt{(N)} = 1.5'$ where $\Delta = 0.15°$ is the angular resolution and $N = 34$ the number of excess events. The systematic uncertainty is of about $2'$. The source position is compatible within errors with the position of Cygnus X-1 and excludes the jet-powered radio nebula at a distance of $\sim 8'$ (see Figure 24).

We have evaluated the source extension by comparing the distribution of excess events as a function of θ^2 to the one predicted by MC simulations. For this we have used a MC standard test sample corresponding to a point-like source, observed in wobble mode, with the same zenith angle distribution as Cygnus X-1 observations and the same analysis and SIZE cuts applied. The results are shown in Figure 25. The detected signal is compatible with a point-like source within statistical uncertainties.

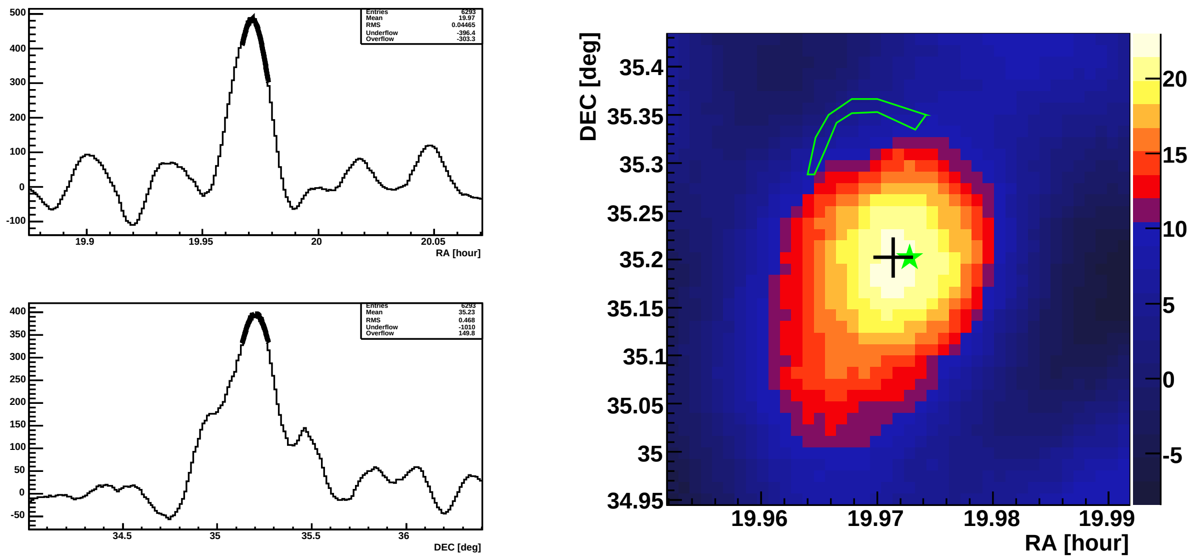

Figure 24: Left plots: RA (top) and DEC (bottom) projections of the Cygnus X-1 sky-map using bands of DEC $= \mathrm{DEC}_0 \pm 0.1^\circ$ RA $=\mathrm{RA}_0 \pm 0.008$ hours, respectively. The thick solid line shows the result of the Gaussian fit to the central part of the distributions. Right: zoomed sky-map centered at the source region. The black cross corresponds to the best fit position and the size of the cross to the systematic and statistical errors added in quadrature. The green star corresponds to the position of Cygnus X-1. The green contour shows the region of the jet-powered radio nebula (See [4]).

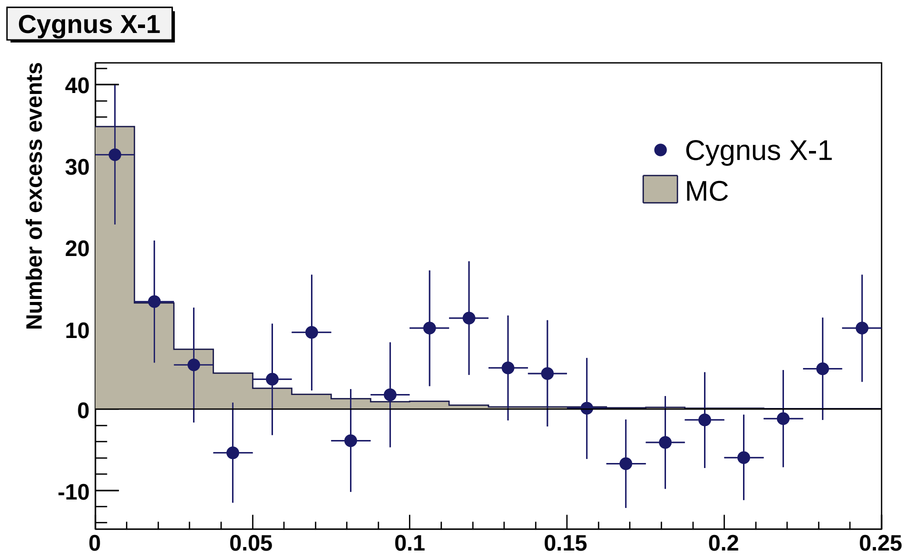

Figure 25: Distribution of excess events as a function of θ^2 for Cygnus X-1 sample 25/09/2006-B compared to MC simulations. The MC test sample is the standard MAGIC MC corresponding to a point-like source, observed in wobble mode, with the same zenith angle distribution as Cygnus X-1 observations and the same analysis and SIZE cuts applied. The two histograms are normalized to the total area.

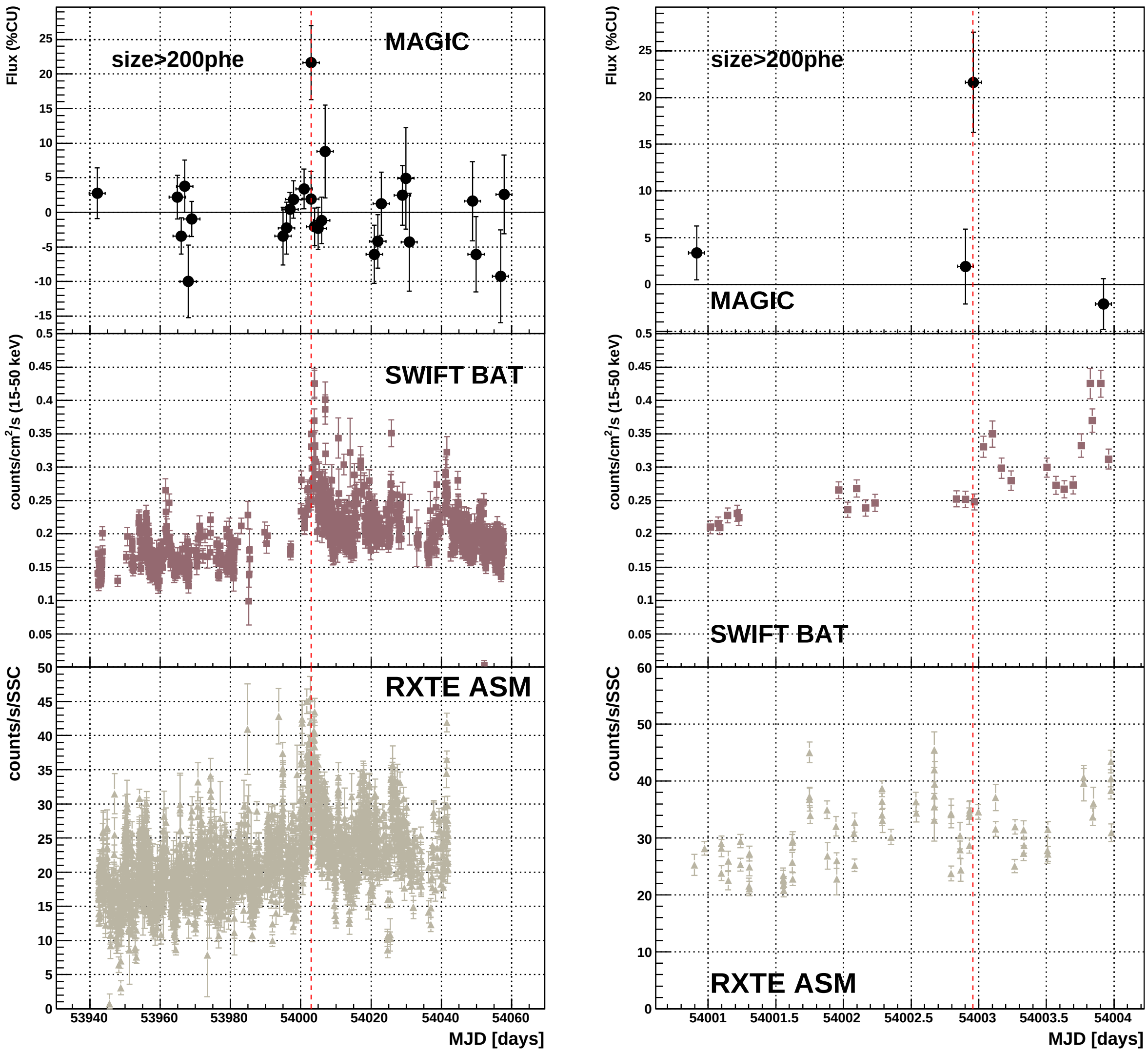

Figure 26: From top to bottom: MAGIC, Swift BAT and RTXE ASM fluxes measured from Cygnus X-1 as a function of the time. The left plots show the whole time spanned by MAGIC observations. The right plots are a zoom around the MAGIC detection. The red line marks the time of the MAGIC detection.

4.4 Correlation with X-ray data

We have compared MAGIC results with public data from SWIFT [17] and ASM [18] (see Figure 26). The left plots show a clear correlation between the time of MAGIC detection with that of the large increase of X-ray fluxes measured by both detectors. A zoom into the region of interest shows that the SWIFT peak has indeed a double-peak structure. MAGIC detection occurs immediately before (about 1.9 hours) the first peak detected by SWIFT (MJD=53003.10). Swift detects a second, even higher peak at MJD=53003.80. MAGIC started an observation at 54003.86, with no positive detection.

On the other hand, INTEGRAL posted an astronomical telegram [19] reporting about the observation of Cygnus X-1 at a historic hard X-ray maximum since INTEGRAL's launch in October 2002.

Between 24-26 September 2006 (MJD 54002-54004) the source showed a more or less constant flux at a level of about 1.5 Crab (20-40 keV) and 1.8 Crab (40-80 keV). On top of this high state, INTEGRAL observes an outburst lasting about 8 hours and reaching a maximum of about 2.0 Crab (20-40 keV) and 2.3 Crab (40-80 keV) in a pointing taken on 25 September 2006 between 20:58 and 21:57 UT (MJD=54003.87-54003.91).

5 Conclusions

We have presented the results obtained from the analysis of the observations of Cygnus X-1 with MAGIC during cycle II. The results show no steady gamma-ray emission above the sensitivity of the instrument, and upper limits of the order of 1-2% Crab have been imposed. A search for periodic signals (using the orbital period) shows evidence for emission in the 0.9-1.0 phase bin, although the data at this phase bin correspond all to the same observation night, and therefore an isolated episode, uncorrelated to the phase bin, cannot be excluded. A search for fast-varying signals have shown evidence (4 SD level) for gamma-ray emission on the observation night 27/09/2006 (starting at MJD=54002.88). We have searched for faster gamma-ray signals in an unbiased way, finding a 4.9 SD signal (4.5 post-trial SD) on the second half of the sample (starting at MJD=54002.93). The signal is energy-distributed with a spectrum with spectral slope -3.4 ± 0.5 and a normalization of $\sim$ 10% Crab at 1 TeV. It is a point-like source, located at a position compatible with that of Cygnus X-1 (excluding the possibility that the signal comes from the nearby radio-emitting ring-like structure). Our signal is correlated in time with a large increase of the X-ray fluxes measured by Swift, RXTE-ASM and INTEGRAL.

References

[1] D. R. Gies and C. T. Bolton, ApJ **260** (1982) 240.

[2] J. M. Miller *et al.*, ApJ **653** (2006) 525.

[3] Stirling et al. MNRAS **327** (2001) 1273.

[4] E. Gallo *et al.*, Nature **436** (2005) 819.

[5] R. Fender *et al.* MNRAS **369** (2006) 603.

[6] M. L. McConnell *et al.* ApJ **543** (2000) 928.

[7] R. C. Hartman *et al.* ApJS **123** (1999) 79.

[8] Physics Working Group on Galactic Sources, "MAGIC observation of Cygnus X-1", proposal for MAGIC's cycle II. Available at:
http://magic.ifae.es/galactic_sources_pwg/MagicGalactic/C-II_files/magic-cygnusX1_v5.pdf

[9] E. Oña-Wilhelmi *et al.*, "Observations under moonlight and twilight with MAGIC", MAGIC-TDAS 06-09.

[10] J. Albert (MAGIC Collaboration) *et al.* "Very high energy gamma ray observations under moonlight and twilight with MAGIC", Astrop. Phys. submitted.

[11] A. Moralejo, "Monte Carlo simulation for data taken after June 2006". MAGIC analysis meeting. Madrid, Nov 2006. Available at:
http://www.gae.ucm.es/ MAGIC/meeting/analysis-premeeting/

[12] T. Li and Y. Ma, ApJ **272** (1983) 317.

[13] W. A. Rolke, A. M. López and J. Conrad, Nucl. Intr. and Meth. **A551** (2005) 593.

[14] M. Rissi, private communication

[15] M. López Moya, private communication

[16] Available at http://magic.pic.es/datacenter/LaPalma/Datacheck/

[17] Available at http://swift.gsfc.nasa.gov/docs/swift/results/transients/CygX-1/

[18] Available at http://heasarc.gsfc.nasa.gov/cgi-bin/xte_weather/xte_lc?source=CYGX1

[19] Astronomical telegram ATEL #911, available at http://www.astronomerstelegram.org/